Journal of Power Sources 646 (2025) 237267

Contents lists available at ScienceDirect

Journal of Power Sources

journal homepage: www.elsevier.com/locate/jpowsour

Bio- and Electrocatalysts for Oxygen Reduction Reaction in Neutral Media: From Mechanisms to Practical Applications

Angelo Tricase [a,b], Mohsin Muhyuddin [c], Benjamin Erable [d], Plamen Atanassov [e], Deepak Pant [f], Carlo Santoro [c], Paolo Bollella [b,g,*]

[a] Department of Pharmacy-Pharmaceutical Science, University of Bari A. Moro, Via E. Orabona 4, 70125, Bari, Italy
[b] Centre for Colloid and Surface Science, University of Bari A. Moro, Via E. Orabona 4, 70125, Bari, Italy
[c] Electrocatalysis and Bioelectrocatalysis Laboratory (EBLAB), Department of Material Science, University of Milano-Bicocca, Building U5, Via Cozzi 55, 20125, Milan, Italy
[d] Laboratoire de Génie Chimique, Université de Toulouse, CNRS, INPT, UPS, Toulouse, France
[e] Department of Chemical & Biomolecular Engineering and National Fuel Cell Research Center, University of California Irvine, Irvine, CA, 92697, USA
[f] Electrochemistry Excellence Centre (ELEC), Materials & Chemistry Unit, Flemish Institute for Technological Research (VITO), Boeretang 200, Mol, 2400, Belgium
[g] Department of Chemistry, University of Bari A. Moro, Via E. Orabona 4, 70125, Bari, Italy

HIGHLIGHTS

- ORR kinetics in neutral medium are slower compared to acidic or alkaline media.
- O_2 can adsorb onto electrocatalyst surfaces through three distinct modes.
- Novel (bio)cathode designs will enhance ORR kinetics in neutral media.

ARTICLE INFO

Keywords:
Oxygen reduction reaction (ORR)
Neutral pH
Platinum group metals (PGM) electrocatalysts
PGM-Free electrocatalysts
Multicopper oxidases (MCOs)
Bacterial ORR-Electrocatalysts

ABSTRACT

Oxygen reduction reaction (ORR) is a key electrochemical process with significant implications at the industrial level from energy conversion/storage to corrosion protection and production of valuable chemicals. Oxygen is also critically involved in biological systems at the level of the respiratory chain, allowing the development of several biomimicking bioelectrochemical devices encompassing microbial fuel cells (MFCs) and enzymatic fuel cells (EFCs) exploited for power generation, organics transformation, water desalination, biosensing and other applications. Many studies on ORR mechanisms in near-neutral environments for potential integration with bioprocesses are currently ongoing with many phenomena still to be explained, especially concerning biotic and abiotic electrocatalysts. This comprehensive review aims at summarizing the state-of-the-art for each electrocatalyst category, namely: noble-metal/transition-metal-based/carbonaceous electrocatalysts, enzymes, and bacterial cells. In particular, the performances are compared based on their ORR mechanisms, quantitatively discussing the practical limitations, and addressing the technological challenges of their integration in sustainable electronics.

1. Introduction

Oxygen reduction reaction (ORR) is a fundamental electrochemical process that underpins the performance of energy conversion systems such as fuel cells and metal-air batteries [1–4]. In neutral media, ORR is particularly relevant for applications requiring biocompatibility and operational stability, including enzymatic fuel cells, microbial fuel cells, and advanced bioelectronic devices [5–8]. However, the kinetics of ORR in neutral conditions are inherently slower compared to acidic or alkaline environments due to reduced proton activity ($[H^+] \sim 10^{-7}$ M) affecting both O_2 adsorption on electrocatalyst surfaces and ORR intermediates stabilization through proton-coupled electron transfer (PCET), such as superoxide (O_2^-) and hydrogen peroxide (H_2O_2)

This article is part of a special issue entitled: Bioelectrochemistry published in Journal of Power Sources.

* Corresponding author. Centre for Colloid and Surface Science, University of Bari A. Moro, Via E. Orabona 4, 70125, Bari, Italy.
E-mail address: paolo.bollella@uniba.it (P. Bollella).

https://doi.org/10.1016/j.jpowsour.2025.237267
Received 30 September 2024; Received in revised form 24 February 2025; Accepted 30 April 2025
Available online 8 May 2025

List of abbreviations

4-ABA	4-aminobenzoic acid
AQS	anthraquinone sulfonate
AuNPs	gold nanoparticles
BESs	bioelectrochemical systems
BET	Brunauer-Emmett-Teller
BNC	heme-copper binuclear center
CcO	cytochrome *c* oxidase
CPA	carbon paper
CPs	conductive polymers
CuBTT	Cu-based complex
DBA	1-dodecylboronic acid
DET	direct electron transfer
DFT	density functional theory
EAB	electroactive biofilms
E_b	binding energy
ECSA	electrochemically active surface area
EFCs	enzymatic fuel cells
EPS	extracellular polymeric substances
ET	electron transfer
GDE	gas-diffusion electrode
GNPs	glyconanoparticles
HBM	hybrid bilayer membrane
IRRAS	infrared reflection absorption spectroscopy
LD-EET	long-distance extracellular electron transport
M-N-C	metal-nitrogen-carbon
MCOs	multicopper oxidases
MFCs	microbial fuel cells
MIC	microbiologically influenced corrosion
MnOOH	manganese oxyhydroxide
MSC	microbial solar cell
MvBOD	bilirubin oxidase
MWCNT	multi-walled carbon nanotube
NI	native intermediate
O-CNTs	oxidized carbon nanotubes
O_2ads	adsorbed O_2
OCV	open circuit voltage
OFGs	oxygen functional groups
ORR	oxygen reduction reaction
OSET	oxygen single-electron transfer
PBSE	1-pyrenebutanoic acid N-hydroxysuccinimide ester
PCET	proton-coupled electron transfer
PDMS	polydimethylsiloxane
PEG	polyethylene glycol
PGM	platinum group metals
PI	peroxy intermediate
Pt	platinum
PTFE	polytetrafluoroethylene
RDS	rate-determining step
RGO	reduced graphene oxide
RHE	real hydrogen electrode
ROS	reactive oxygen species
SAM	self-assembled monolayer
SS	stainless steel
T3μ_2OH bridge	T3 copper hydroxy bridge
Ti	titanium
TM-N-C	transition metal-nitrogen-carbon
TNC	trinuclear copper center
TPI	three-phase interface
ZNCs	silicalite-1 nanocrystals

[9–11]. Additionally, O_2 adsorption is influenced by the electrostatic interaction between O_2 and the surface charge of the electrocatalyst [12,13]. At neutral pH, many electrocatalysts exhibit reduced surface charge densities compared to acidic or alkaline conditions, which weakens the electrostatic attraction and diminishes O_2 binding to the active sites [14,15]. Furthermore, H_2O molecules, abundant in neutral media, can occupy active sites, blocking O_2 adsorption and reducing the availability of sites for ORR [16,17]. This competition is particularly pronounced on electrocatalysts with hydrophilic surfaces or poor O_2 selectivity [18]. However, protonation is also essential for stabilizing superoxide (O_2^-) and hydrogen peroxide (H_2O_2) as intermediates, because O_2^- is typically converted to the hydroperoxyl radical ($HO_2^{\cdot}$) further converted to H_2O_2 [19]. Neutral pH slow these protonation reactions leading to the accumulation of unstable intermediates [20]. This impairs the overall reaction kinetics and shifts ORR mechanism towards less efficient $2e^-$ pathway, where H_2O_2 is produced as the final product instead of H_2O [21,22].

Addressing these challenges is crucial for developing energy-efficient and environmentally friendly systems capable of operating in mild or biologically relevant conditions [23]. In particular, noble-metal electrocatalysts, such as platinum or platinum group metals, PGMs), are widely regarded as “standards” due to their high activity and selectivity for the $4e^-$ reduction pathway, which directly converts O_2 to H_2O [24]. However, their high cost and limited availability have spurred interest in alternative materials. Transition metal-nitrogen-carbon (TM-N-C) electrocatalysts have emerged as promising non-precious alternatives, offering high catalytic activity, structural versatility, and economic feasibility [25]. Similarly, carbon-based materials, such as graphene and nitrogen-doped carbons, have gained attention for their abundance and adaptability, although they often favor the $2e^-$ pathway, leading to the production of H_2O_2 [26]. Biological catalysts, including enzymes like multicopper oxidase (MCOs, e.g., laccases, bilirubin oxidases etc.), provide excellent selectivity for the ORR in neutral conditions but suffer from stability and operational challenges [27,28]. Artificial enzymes (e.g., supramolecular electrocatalysts) represent an innovative approach by mimicking enzymatic active sites to achieve enhanced catalytic performance [29]. Additionally, electrogenic bacteria capable of extracellular electron transfer, such as *Geobacter sulfurreducens*, have opened new avenues for ORR in microbial fuel cells (MFCs) and other bioelectrochemical applications [30–32]. Mechanistic studies from the past five years have elucidated the roles of molecular adsorption, electron transfer, and intermediate stabilization on these electrocatalysts, offering valuable insights for optimizing ORR performance in neutral media [11,33].

Notably, O_2 adsorption onto electrocatalyst surfaces is a crucial step in ORR, as it initiates the subsequent reduction processes [24,34]. The process begins with the physical adsorption through weak interactions, followed by chemisorption, where O_2 molecules form stronger bonds with the active sites on the electrocatalyst surface [18]. For noble-metal electrocatalysts like platinum (Pt/C), O_2 typically binds in configurations that weaken the O-O bond, facilitating electron transfer and enabling the formation of reactive intermediates such as superoxide (O_2^-) and hydroperoxyl (HO_2) [35]. These intermediates are then efficiently reduced to H_2O via a kinetically favorable pathway. In contrast, non-noble metal and carbon-based electrocatalysts often have weaker O_2 adsorption due to differences in electronic structure, which can result in partial reduction pathways and increased stabilization of intermediates [36–38]. Enzymatic and microbial electrocatalysts employ distinct adsorption mechanisms, where O_2 interacts with active sites such as metal centers or enzyme complexes, often enabling specific reaction pathways [39,40]. Factors such as proton concentration, surface charge, and water competition also influence the adsorption process at

neutral pH, impacting the efficiency and selectivity of the ORR [41]. Understanding and optimizing these adsorption mechanisms are critical for improving catalytic performance in neutral environments.

Moreover, detecting superoxide (O_2^-) and hydrogen peroxide (H_2O_2) as intermediates of the ORR at neutral pH is critical for understanding the reaction mechanism and improving electrocatalyst efficiency [37,42,43]. These intermediates play a key role in determining whether the ORR proceeds via the $2e^-$ or $4e^-$ pathway, with the latter being more desirable for the direct reduction of O_2 to H_2O [9]. Accumulation of O_2^- or H_2O_2 indicates inefficient electrocatalysis leading to energy losses and potential degradation of the electrocatalyst [44,45]. For noble-metal electrocatalysts, such as platinum, optimal O_2 binding helps suppress intermediate formation. Non-noble metal and carbon-based electrocatalysts can be tuned by introducing dopants, such as nitrogen or transition metals, to enhance active site reactivity and improve intermediate reduction. Additionally, coupling electrocatalysts with proton donors or facilitating PCET can promote the conversion of intermediates into H_2O [46].

Recently, Santoro et al. have summarized recent findings on ORR mechanisms over inorganic electrocatalysts, enzymatic systems, and bacterial platforms, emphasizing electron transfer (ET) pathways, limitations, and specific applications in bioelectrochemical systems (BESs). Future directions and challenges for ORR in circumneutral pH environments focus on bridging the gap between fundamental mechanistic insights and practical implementation in sustainable technologies [47].

Differently, this review focuses on two critical aspects of ORR: O_2 adsorption and the stabilization of intermediates, particularly superoxide (O_2^-) and hydrogen peroxide (H_2O_2). It examines the mechanistic challenges associated with O_2 binding to electrocatalyst surfaces and the subsequent reduction pathways, emphasizing the interplay between adsorption efficiency and intermediate stabilization across various electrocatalysts. Noble-metal, non-noble-metal, and carbonaceous electrocatalysts are compared in terms of their ability to promote efficient O_2 adsorption and manage intermediates, with a focus on optimizing binding energies and electrocatalytic performance. Enzymatic and bacterial systems are explored for their unique mechanisms of intermediate stabilization and their implications for bioelectrochemical systems (BESs). The discussion highlights the importance of designing electrocatalysts that can effectively adsorb O_2 while minimizing the accumulation of reactive intermediates, thereby favoring the direct reduction of O_2 to H_2O, as shown in Fig. 1. The review concludes by addressing strategies to enhance ORR performance at neutral pH through mechanistic insights into adsorption and intermediate control, paving the way for advancements in sustainable energy and bioelectronic applications.

2. Oxygen reduction reaction (ORR): adsorption mechanisms and limiting steps

O_2 molecules can adsorb onto electrocatalyst surfaces through three distinct modes: Griffith-type mode, where O_2 binds either via side-on coordination to a single electrocatalytic site or via end-on interaction with a single electrocatalytic site; Pauling-type mode, where O_2 attaches end-on to a single electrocatalytic site; and Yeager-type mode, where O_2 forms a side-on bridge across two adjacent electrocatalytic sites [48,49]. O_2 adsorption mechanisms play a key role in addressing ORR, as shown in Fig. 2.

Particularly, the Griffith-type adsorption mechanism relies on the formation of electrocatalyst (low energy state)-O_2 bond due to weak chemical bonds or van der Waals interactions with the surface atoms. O_2 molecule remains intact with little distortion or activation. The mechanism does not involve a substantial weakening of the O-O bond, which limits its ability to facilitate subsequent reduction steps in ORR. While the Griffith-type adsorption mechanism is thermodynamically favored, it is generally not effective for catalyzing ORR because it fails to activate O_2 for the reduction process. Stronger binding or dissociation of O_2 is typically required to initiate PCET processes that are essential for ORR [50,51].

Pauling end-on adsorption mechanism relies on electrocatalyst-O_2 interaction through a single oxygen atom. This adsorption mode retains the O_2 molecular structure while moderately weakening the O-O bond, facilitating its subsequent reduction. The end-on configuration typically supports the associative pathway of ORR, enabling the formation of intermediates like superoxide (O_2^-) and hydroperoxyl radical ($HO_2^{\cdot}$) before the complete reduction to H_2O [52]. The mechanism begins with the adsorption of O_2 on the electrocatalyst surface, where an electron is transferred to form O_2^- intermediate (eq. (1)):

$$O_2 + e^- \rightarrow O_2^- \quad (1)$$

The adsorbed O_2^- is then protonated to form $HO_2^{\cdot}$ (eq. (2)):

$$O_2^- + H^+ \rightarrow HO_2^* \quad (2)$$

Subsequent electron and proton transfers reduce $HO_2^{\cdot}$ to OH* and finally to H_2O, eq. (3):

$$HO_2^* + e^- + H^+ \rightarrow H_2O + OH^* \quad (3)$$

This pathway is especially efficient on noble-metal electrocatalysts, such as platinum, due to their ability to provide optimal binding energy for O_2, ensuring activation without excessive stabilization of intermediates. On these electrocatalysts, the end-on mechanism predominantly drives the $4e^-$ pathway, directly reducing O_2 to H_2O (eq. (4)):

$$O_2 + 4H^+ + 4e^- \rightarrow 2H_2O \quad (4)$$

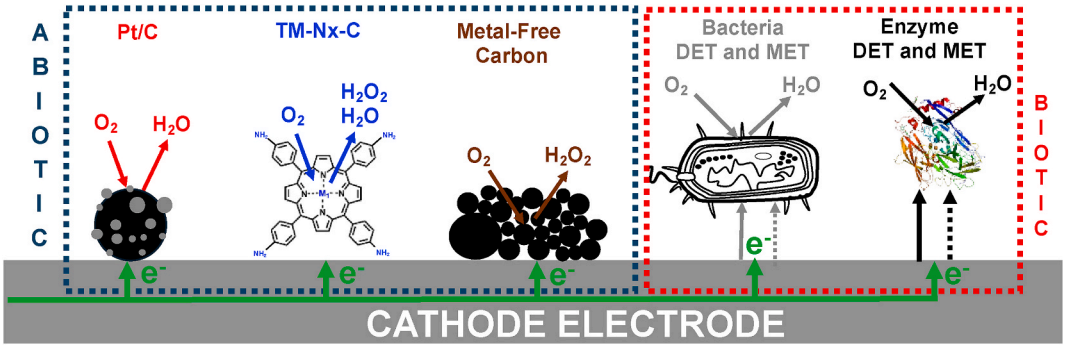

Fig. 1. Oxygen reduction reaction schematic occurring over abiotic and biotic electrocatalysts. From left to right: ORR over Pt/C electrocatalyst; over Fe-N-C electrocatalyst, over carbonaceous-based metal-free electrocatalyst, ORR in the presence of bacteria through direct and mediated electron transfer, ORR using enzymes through direct and mediated electron transfer.

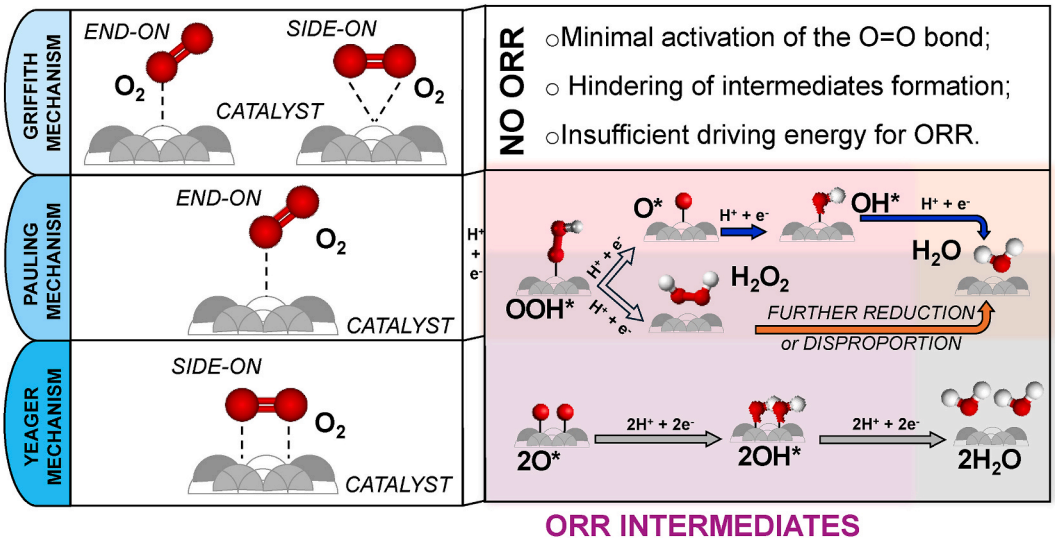

Fig. 2. Correlation between oxygen adsorption mechanism and oxygen reduction reaction (ORR): (i) Griffith mechanism does not favor ORR, (ii) Pauling mechanism favors 4e⁻ associative mechanism for ORR (blue pathway), and (iii) Yeager mechanism favors the 2e⁻ associative mechanism for ORR (orange pathway) and dissociative ORR (grey pathway). (For interpretation of the references to colour in this figure legend, the reader is referred to the Web version of this article.)

However, on electrocatalysts with weaker oxygen binding, such as carbon-based materials, the same mechanism can lead to a 2e⁻ pathway, where the reduction produces H_2O_2 (eq. (5)):

$$O_2 + 2H^+ + 2e^- \rightarrow H_2O_2 \quad (5)$$

In the Yeager-type mechanism, O_2 binds to two adjacent electrocatalytic sites, creating a stronger interaction compared with other adsorption mechanisms. This binding geometry exerts substantial strain on the O-O bond, which facilitates its cleavage (*dissociative pathway*) or activation (*associative pathway*) [53,54].

In the dissociative pathway, the O-O bond breaks immediately upon adsorption, producing two oxygen atoms adsorbed on the electrocatalyst surface (eq. (6)):

$$O_2 \rightarrow O^* + O^* \quad (6)$$

Each adsorbed oxygen atom (O*) is then reduced independently (eqs. (7) and (8)):

$$O^* + H^+ + e^- \rightarrow OH^* \quad (7)$$

$$OH^* + H^+ + e^- \rightarrow H_2O \quad (8)$$

The Yeager-type adsorption strongly supports the dissociative pathway due to its ability to destabilize and break the O-O bond. Electrocatalysts such as single atoms transition metals coordinated with nitrogen (e.g., Fe-N-C or Co-N-C) commonly undergo this mechanism, as the adjacent active sites in these materials provide the necessary configuration for bridge adsorption and bond cleavage [55].

Enzymatic and biological electrocatalysts, such as laccases or artificial enzymes, primarily undergo Pauling end-on adsorption mode, where O_2 binds at active metal centers, such as copper or iron, within the enzymatic electrocatalytic site. These systems are highly selective for the 4e⁻ pathway, reducing O_2 to H_2O avoiding the accumulation of intermediates [56]. In bacterial systems, extracellular electron transfer mechanisms can involve mixed adsorption modes, where O_2 and its intermediates interact with protein-bound or surface-adsorbed active sites [57].

At circumneutral pH, a slow protonation can lead to the accumulation/desorption of intermediates (causing catalyst degradation), increasing the risk of side reactions or incomplete reduction pathways that produce H_2O_2 instead of H_2O [58,59].

Recently, Briega-Martos and his co-workers detected O_2^- intermediates by using *in situ* infrared reflection absorption spectroscopy (IRRAS) onto platinum (111) electrode in an O_2-saturated solution at pH 5.5, proving that platinum can stabilize superoxide intermediates under mildly acidic to neutral conditions [16,19]. The superoxide anion has a pKa of around 4.8, meaning that at neutral pH, it predominantly exists in its deprotonated form, with less than 1 % present as its conjugate acid, hydroperoxyl radical ($HO_2^{\cdot}$) [60]. However, excessive stabilization of O_2^- can be detrimental, leading to the accumulation of reactive oxygen species (ROS) and potential electrocatalyst degradation. Therefore, the design of ORR electrocatalysts for neutral pH applications should balance: optimal binding energy (sufficient binding energy to stabilize O_2^- to enable its reduction without excessive accumulation), efficient proton transfer (promote the conversion of O_2^- to $HO_2^{\cdot}$), and prevention of side reactions (avoid ROS species formation) [61].

For instance, the degradation of Fe-N-C electrocatalysts during the ORR at neutral and acidic pH is primarily caused by Fe demetalation, protonation of nitrogen groups, carbon corrosion, and reactions with H_2O_2 hydrogen peroxide, an intermediate of ORR. H_2O_2 reacts with Fe species through Fenton-like reactions, generating ROS species that oxidize the carbon surface, reducing the electrocatalytic efficiency and increasing hydrophilicity, leading to micropore flooding. These effects are more pronounced under acidic conditions, while neutral/alkaline conditions show resistance to degradation, possibly due to slower carbon oxidation. Recently, Bae et al. investigated the pH-dependent behavior of Fe-N-C catalysts in the presence of H_2O_2 and its implications for electrocatalyst durability, proving that at neutral/alkaline pH this effect can be mitigated [62].

Armillotta et al. mechanistically demonstrated that the most stable configuration of hydroperoxyl binding to the Co metal center (Co-OOH) has a binding energy of 6.12 eV (*ab initio* calculation) [63]. Stabilization occurs through three mechanisms: electron transfer from the CoTPyP macrocycle to O_2H, strong hydrogen bonding between O_2H and H_2O, and long-range van der Waals interactions involving adjacent groups (Fig. 3). Hydroperoxyl binding alone also induces a Co oxidation state change from +2 to +3, but the addition of water restores the Co oxidation state to +2 while further stabilizing the complex. Both Co-OOH and a less stable Co-OHO configuration could coexist, depending on environmental conditions. Hence, this suggests that the selectivity between the 2e⁻ and 4e⁻ ORR pathways may be influenced by the specific configuration of the hydroperoxyl ligand at the electrocatalyst's active site, due to charge transfer, chemical interactions, dipole effects, and hydrogen bonding (or solvation) phenomena [64].

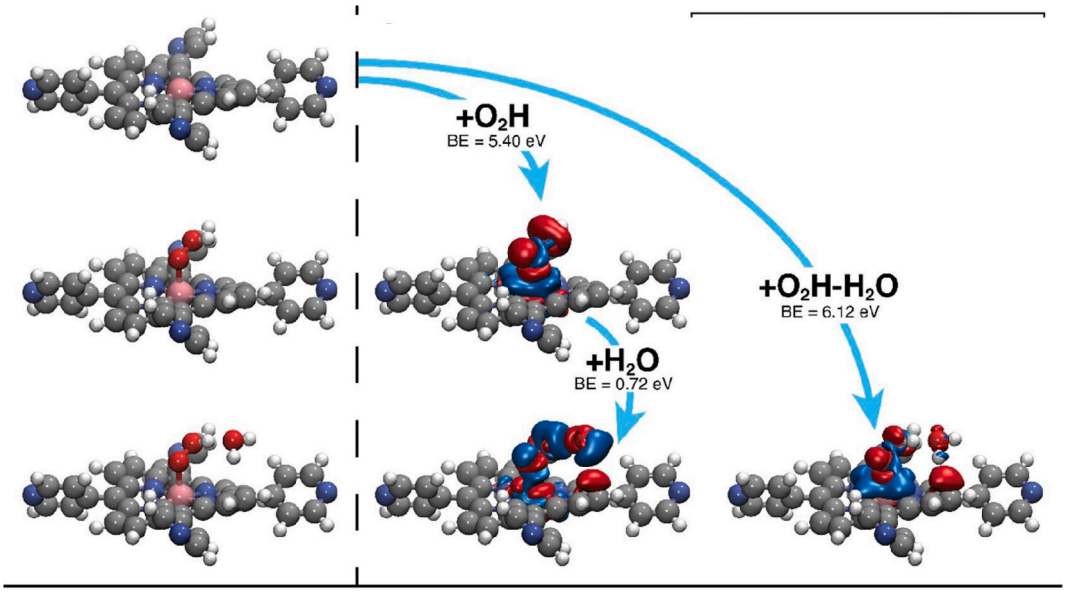

Fig. 3. *Ab initio* analysis showing that the adsorption of O_2H and H_2O on the CoTPyP/graphene system has a minimal effect on its structure, apart from a slight upward shift of the Co atom by 0.16 Å. The bonding causes a redistribution of electron density in the O_2H-H_2O/CoTPyP/GR system, as visualized through electron density isosurfaces. Reproduced with permission of American Chemical Society from Ref. [63].

Integrating *in-operando* spectroscopic techniques with *ab initio* calculations will significantly advance the understanding of ORR mechanisms, enabling the design and optimization of electrocatalysts towards efficient ORR [65–68].

3. Metal-based, transition-metal-based single atoms (TM-N-C) and carbonaceous-based electrocatalysts for ORR at neutral pH

Nørskov et al. discovered that the adsorption of intermediate species, such as O and OH, plays a crucial role in the ORR on metal electrocatalysts [69,70]. Metal-based electrocatalysts can be efficiently optimized by combining experimental and theoretical methods (mainly density functional theory (DFT)) [49]. The direct cleavage of the O-O bond during ORR on the cathode is challenging due to the high reorganization energy of O_2 [71]. Additionally, the unpaired electrons in the π^* orbital of O_2 enable it to accept electrons, weakening the O-O bond. Electrons transferred from the metallic active site to the π^* orbital, along with protons from the anode, generate reactive oxygen species (*OOH, *O, and *OH) on the electrocatalyst surface [72]. The binding energy (E_b) of these intermediates is a critical factor in determining ORR activity, making it a key descriptor for electrocatalyst efficiency [73]. Modifying the binding energy of ORR intermediates through surface engineering is, therefore, crucial for improving electrocatalyst performance. Using calculated E_b values for different electrocatalysts, a Volcano plot was constructed to relate E_b to ORR activity (Fig. 4A). Electrocatalysts on the right side of the plot, which have strong oxygen binding, experience limitations in activity due to slow proton and electron transfer to the *O or *OH intermediates. Conversely, electrocatalysts on the left side, with weak O_2 binding, are constrained by proton and electron transfer to O_2, followed by either the associative or dissociative pathways (*shown in the previous section*) [74].

Metals with slightly lower oxygen binding energy than pure platinum (Pt) have the potential to achieve higher ORR rates. DFT calculations reveal that Pt alloys with elements such as Ni, Co, Fe, and Cr exhibit reduced O_2 binding energies compared to pure Pt, while the decreasing in OH binding energy on these alloys is less pronounced. For instance, DFT calculations indicate OH and O binding energies (ΔE_{OH}, ΔE_O) as follows (Fig. 4A): (1.15 eV, 1.89 eV) for Pt over Ni, (1.06 eV, 2.00 eV) for Pt over Co, and (0.85 eV, 2.06 eV) for Pt over Fe. In contrast, on pure Pt, these values are (1.05 eV, 1.57 eV). A Pt layer deposited onto $Pt_3Co(111)$ has an oxygen binding energy 0.38 eV lower than pure Pt (111), leading to increased reactivity. These studies highlight that Pt layers on such alloys outperform pure Pt in ORR activity [69].

However, defects on Pt surfaces, such as those on Pt(110), tend to bind O_2 more strongly (by 0.5 eV) than flat surfaces, reducing the activity. It is important to note that surface activity is not solely determined by O_2 binding energy but also depends on OH binding energy, as both are interconnected. O_2 and OH binding energies are generally linearly correlated for elemental surfaces. However, new electrocatalysts can be tailored with a non-linear correlation between O and OH binding energies [69].

Recently, Thorarinsdottir et al. reported the synthesis of disk-shaped silicalite-1 nanocrystals (ZNCs, $d = 197 \pm 16$ nm) able to entrap gaseous O_2 dissolved in solution [75]. In the presence of ZNCs 6.7 vol%, the O_2 adsorption capacity increased up to 3.8×10^2 mM bar^{-1} at 20 °C, which is 2 orders of magnitude higher than O_2 adsorption capacity in phosphate buffer solution at pH 7. Pt/C modified electrode reported a plateau current density of 4.5 mA cm^{-2} as a result of O_2 mass transport limitations. After a gradual increase of ZNCs mass in solution from 25.0 to 122.7 mg mL^{-1}, the ORR current density increased by 3.8–3.9 times reaching 17.5 mA cm^{-2} as plateau current density. Electrokinetic modeling reveals that microporous water significantly enhances ORR electrocatalysis at pH 7 (enhancing $[H^+]$ concentration to favor PCET within ORR). The model predicts O_2 diffusion via a hopping mechanism between ZNCs, following a chemical step preceding an electrochemical step (CE mechanism). In phosphate-buffered water, the theoretical maximum current density is 27.4 mA cm^{-2}, but experimental measurements without ZNCs show only 4.5 mA cm^{-2}. Adding 6.7 vol% ZNCs increases the current density to 17.5 mA cm^{-2}, reducing oxygen mass transport limitations (Fig. 4B). This approach extends the ORR regime and provides a valuable framework for designing advanced ORR electrocatalysts.

Similarly, Lv and co-workers enhanced the performance of the Pt/C cathode at a nearly neutral pH by adding the polyoxoanion $[Fe_{28}(\mu_3\text{-}O)_8(L\text{-}(-)\text{-}tart)_{16}(CH_3COO)_{24}]^{20-}$ with phosphate buffer solution [76]. Particularly, Fe_{28} enhances oxygen uptake and solubility in aqueous electrolytes, contributing to improved ORR performance. Time-resolved O_2 sensing revealed that Fe_{28} solutions had a faster O_2 uptake rate (12.6 μmol L^{-1} s^{-1}) compared to PBS solutions (8.0 μmol L^{-1} s^{-1}), while both showed similar O_2 saturation levels (~750 μmol L^{-1}). This indicates that

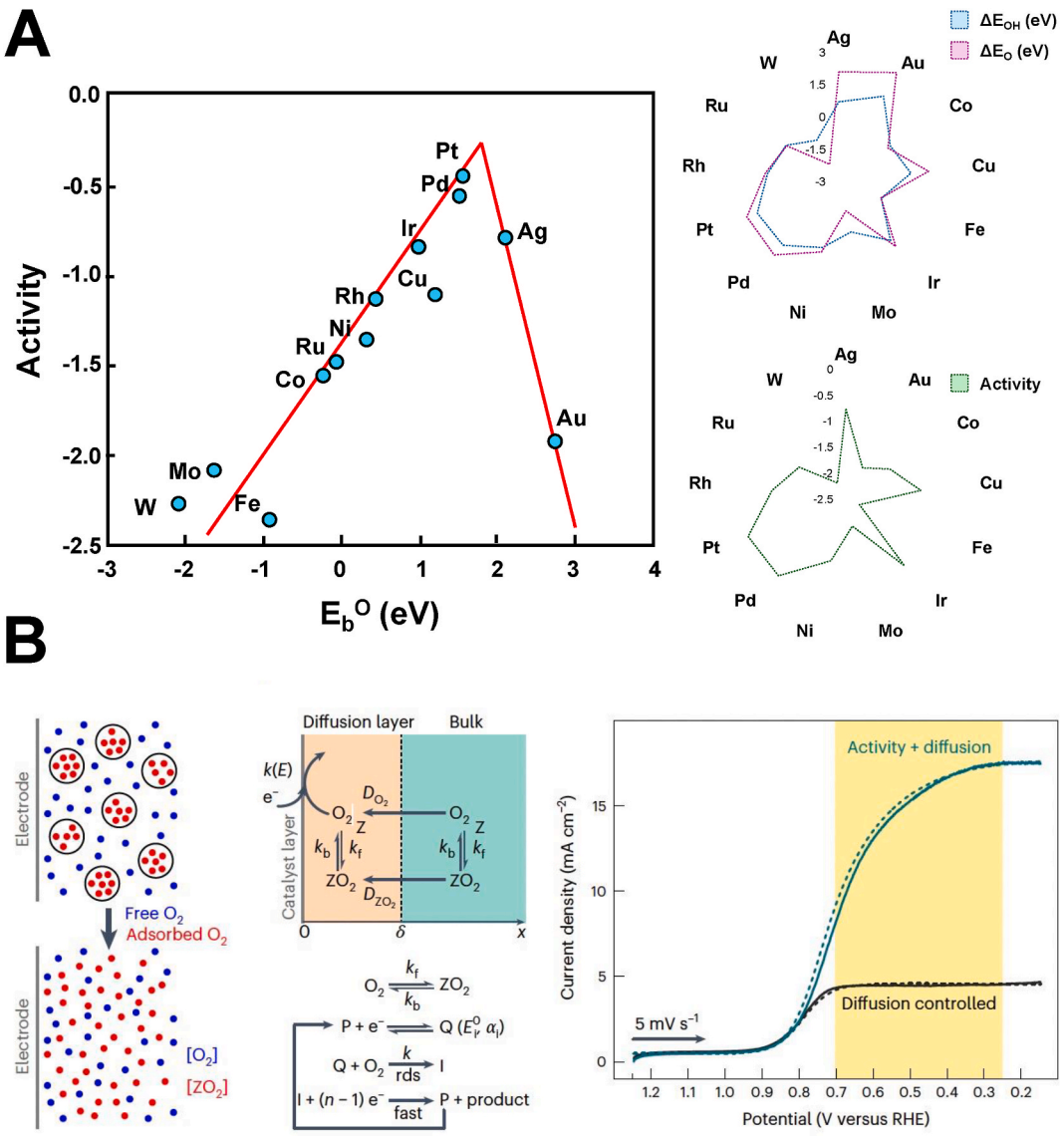

Fig. 4. **(A)** Volcano plot correlating ORR activity for different metals vs. O_2 energy binding (E_b^O) and Radar plots correlating OH and O binding energies (ΔE_{OH}, ΔE_O) and ORR activity. **(B)** A detailed electrokinetics model for oxygen reduction reaction (ORR) in the presence of silicalite-1 nanocrystals (ZNCs) describes the equilibrium between free oxygen molecules in solution and those adsorbed within the nanocrystals. This system follows a CE-type (chemical-electrochemical) mechanism, where adsorbed oxygen molecules must desorb prior to their reduction at the electrode. Experimental results, such as RDE voltammograms in phosphate-buffered water at pH 7.0, demonstrate that incorporating ZNCs significantly expands the potential range for activity-dominated current densities. This extended range, supported by electrokinetics modeling, highlights the role of microporous materials in enhancing ORR efficiency through optimized oxygen diffusion and reaction pathways. Panel A partially adopted with permission of American Chemical Society from Ref. [69]. Panel B adopted with permission of SpringerNature from Ref. [75].

Fe_{28} improves gas-to-liquid mass transfer, likely driving the enhanced ORR activity. PBS-Fe_{28} solution exhibited more positive onset potentials (E_{ONSET} = 0.97 V vs. RHE) compared to the phosphate solution (E_{ONSET} = 0.89 V vs. RHE). Similarly, the half-wave potentials ($E_{1/2}$) followed the same trend, with $E_{1/2}(Fe_{28})$ at 0.84 V vs. RHE and $E_{1/2}$(PBS) at 0.74 V vs. RHE. Additionally, Tafel slope analysis showed that Fe_{28} solutions had lower kinetic barriers for ORR (106.6 mV dec^{-1}) compared to the PBS solution (136.6 mV dec^{-1}). Pt/C modified electrode reported a plateau current density of 5.8 mA cm^{-2} at 0.5 V vs. RHE as a result of improved gas-to-liquid mass transfer.

The prohibitive cost of noble metals such as palladium and platinum required for ORR in any type of fuel cell cathode has hindered their widespread adoption. Wu et al. quantitatively studied the synthesis and performance of a novel $Pd_3CuFe_{0.5}$ aerogel electrocatalyst, fabricated using self-assembly and lyophilization techniques with a mild reducing agent [77]. The resulting material exhibits a high Brunauer-Emmett-Teller (BET)-specific surface area of 75.19 m^2 g^{-1}, indicative of its extensive 3D network structure. Electrochemical performance tests revealed that the $Pd_3CuFe_{0.5}$ aerogel achieves a high ORR $E_{1/2}$ potential of 0.92 V versus RHE, surpassing conventional electrocatalysts such as Pt/C. Furthermore, the aerogel demonstrates a limiting current density of 7.6 mA cm^{-2}, a critical metric indicating its ability to support high reaction rates. Long-term stability assessments show that the ORR activity decreases by only 4.9 % after 16,000 s of operation, highlighting its superior durability compared to noble-metal-based alternatives. The aerogel also exhibits excellent cycling stability, maintaining performance over 120 h at a charge/discharge current density of 10 mA cm^{-2}, making it a viable option for practical fuel cell applications.

At neutral pH, precious-metals electrocatalysts produce low power

output and are often poisoned by anions that deactivate the surface of Pt/C electrocatalysts [16,78–80]. Alternatively, metals, either precious or non-precious, can be combined in structures TM-N-C to improve both electrocatalytic performance and durability compared to Pt/C electrocatalysts [21,81–85].

Liang et al. reported on the incorporation of Cu nanoclusters into Fe—N—C electrocatalysts that significantly enhance ORR performance by improving the electronic structure and reaction kinetics without altering the rate-determining step (RDS) [86]. In neutral pH (0.1 M PBS), the electrocatalyst achieves an $E_{1/2}$ of 0.84 V and a kinetic current density of 68 mA cm^{-2}, demonstrating superior activity compared to controls. Cu nanoclusters donate electrons to Fe—N_4 active sites, redistributing charge density and increasing electron transfer rates. Additionally, they modulate the spin state of Fe, enhancing reactivity by increasing the spin population. While the RDS in neutral media remains the formation of O_2^- intermediate, Cu clusters accelerate this step by facilitating faster electron dynamics. This synergistic interaction not only boosts ORR activity but also improves stability, with no performance degradation observed after 30,000 durability cycles.

Similarly, Fe,Cu/N-C electrocatalyst demonstrates superior ORR performance in neutral media (0.1 M PBS), achieving an $E_{1/2}$ of 0.73 V vs. RHE, significantly outperforming Pt/C ($E_{1/2}$ = 0.63 V) and single-metal electrocatalysts such as Fe/N-C ($E_{1/2}$ = 0.50 V) and Cu/N-C ($E_{1/2}$ = 0.45 V). It also delivers a high kinetic current density of 15 mA cm^{-2}, which is 10, 20, and 3.3 times greater than Fe/N-C, Cu/N-C, and Pt/C, respectively [87]. The electrocatalyst exhibits remarkable durability, retaining over 86 % of its initial current after 40,000 s of continuous operation, and follows a nearly complete 4e^- pathway with minimal H_2O_2 production (less than 2.5 %), highlighting its efficiency. The superior ORR activity arises from the synergistic interaction between Fe and Cu atoms, which enhances the electronic structure and facilitates reaction kinetics. The introduction of Cu induces a transition of Fe from a low-spin to a medium-spin state, increasing the number of unpaired 3d electrons and enhancing orbital interactions with oxygen intermediates. Additionally, Cu promotes charge redistribution and optimizes electron transfer, as indicated by increased Bader charge transfer to O_2 and *OH species. The reaction follows a tandem mechanism, where Fe sites drive the initial adsorption and transformation of O_2 into *OOH and *O intermediates, while Cu sites accelerate *OH desorption, overcoming limitations associated with single-metal electrocatalysts. Furthermore, the optimized bond strength and reduced activation barriers, aided by the dual active centers, ensure faster reaction kinetics, making Fe, Cu/N-C a highly effective and durable electrocatalyst for neutral pH applications.

Moreover, a comprehensive quantitative comparison to assess the ORR performance of catalysts is below summarized (last five years, Table 1), highlighting variations in their electron transfer pathways, kinetic currents, and $E_{1/2}$. These metrics are critical for evaluating electrocatalytic efficiency, particularly at neutral pH, where ORR performance is typically constrained by sluggish reaction kinetics [86,88], [128]

Most electrocatalysts operate via a 4e^- pathway or 2 + 2 e^-, ensuring efficient O_2 reduction to H_2O. Exceptions include 2e^- pathway electrocatalysts such as CoPc-6wt%/o-SWCNT-2 (n = 2, kinetic current = 45.0 mA cm^{-2}, $E_{1/2}$ = 0.73 V) and Cu-tmpa (n = 2, kinetic current = 3.8 mA cm^{-2}, $E_{1/2}$ = 0.31 V). While the 2e^- pathway is selective for H_2O_2 production, these electrocatalysts generally show lower $E_{1/2}$ and kinetic currents, reflecting limited overall ORR activity. In contrast, FeCu/N-C, Fe1/DNC, and Ni–Co–Mn oxide, which achieve a 4e^- pathway, exhibit the highest kinetic currents of 68.0 mA cm^{-2} and $E_{1/2}$ values ranging from 0.70 to 0.84 V, reflecting their superior electrocatalytic activity and full reduction capability. Electrocatalysts like FeCu/N-C, Fe1/DNC, and Ni–Co–Mn oxide achieve exceptional kinetic currents of 68 mA cm^{-2}, significantly outperforming others such as Fe-N-C (3.0–5.4 mA cm^{-2}) or FeAzPc-CNT (3.2 mA cm^{-2}). The higher kinetic currents can be attributed to structural properties, including optimized porosity and the

Table 1
Comparison of various ORR metal-based, transition-metal-based single atoms (TM-N-C) and carbonaceous-based electrocatalysts considering the number of electrons transferred (n), kinetic current at 0.7 V vs. RHE (mA cm^{-2}), and half-wave potential ($E_{1/2}$) (V vs. RHE). Abbreviations: Ca_2FeRuO_6 (Calcium Iron Ruthenium Oxide), Co-C (Cobalt-Carbon), Co/HNC (Cobalt Hybrid Nitrogen-Carbon), Co/NCA (Cobalt/Nitrogen-Carbon Alloy), CoNC@AC-850 (Cobalt-Nitrogen-Carbon@Activated Carbon), Co-N/C fiber (Cobalt-Nitrogen/Carbon Fiber), CoPc-6wt%/o-SWCNT-2 (Cobalt Phthalocyanine-6wt% on Single-Walled Carbon Nanotubes), CuBPS (Copper-Based Porous Structure), Cu/NCNSs (Copper/Nitrogen-Doped Carbon Nanosheets), CuNSC-3 (Copper/Nitrogen-Sulfur-Carbon), Cu-tmpa (Copper-Tetramethylphenylporphyrin), Fe0.05-N@MOF (Iron-Nitrogen@Metal-Organic Framework), Fe1/DNC (Iron/Nitrogen-Doped Carbon), Fe1/d-CN (Iron-Doped Carbon Nitride), Fe2P/FeNPC (Iron Phosphide/Iron-Nitrogen-Phosphorus-Carbon), FeAzPc-CNT (Iron-Azaphthalocyanine-Carbon Nanotube), Fe-Co-LT (Iron-Cobalt-Layered-Transition Metal Catalyst), FeCo-FePc/NTu-CNsh (Iron-Cobalt-Iron Phthalocyanine/Nanotube Carbon Nitride), FeCo-NC (Iron-Cobalt-Nitrogen-Carbon), FeCu/N-C (Iron-Copper/Nitrogen-Carbon), Fe,Cu/N-C (Iron and Copper/Nitrogen-Carbon), FeMn PDA-900 (Iron-Manganese-PolyDopamine-900 °C), Fe-N-C (Iron-Nitrogen-Carbon), Fe-N-C cig (Iron-Nitrogen-Carbon derived from cigarette but), Fe-NC(Zn^{2+}) (Iron-Nitrogen-Carbon-Zinc), FeN_4-Cu (Iron-Nitrogen-Copper), FeNSC-ZM (Iron-Nitrogen-Sulfur-Carbon-ZM), Fe/Fe_3C@FeNG-1000 (Iron/Iron Carbide@Iron-Nitrogen-Graphene-1000 °C), Fe@G-800/100 (Iron@Graphene-800/100 °C), FeRPM_BP (Iron-RPM-Black Phosphorus), FeSNC-3 (Iron-Sulfur-Nitrogen-Carbon), Fe-SA/PNC (Iron-Single-Atom/Porous Nitrogen-Carbon), IrP_2@PC-0.96 (Iridium Phosphide@Porous Carbon), $MnFe_2O_4$/AC (Manganese-Iron Oxide/Activated Carbon), Ni–Co–Mn oxide (Nickel-Cobalt-Manganese Oxide), P/Fe/N-SS (Phosphorus/Iron/Nitrogen-Stainless Steel), PT-MnN_4 (Platinum-Manganese-Nitrogen-4), and Fe/N/C-50 (Iron/Nitrogen-Carbon-50).

Catalysts	n. electrons	Kinetic current density (mA cm^{-2}) @ 0.7 V vs. RHE	$E_{1/2}$ (V vs. RHE)	Ref.
CoPc-6wt%/o-SWCNT-2	2	45.0	0.73	[88]
Fe,Cu/N-C	4	15.0	0.73	[89]
FeCu/N-C	4	68.0	0.84	[86]
Fe2P/FeNPC	4	n.a.	0.70	[90]
Fe1/DNC	4	68.0	0.70	[91]
Cu-tmpa	2	3.8	0.31	[92]
Fe/Fe_3C@FeNG-1000	2	1.2	0.62	[93]
Fe-N-C	4	3.0	0.85	[94]
CuNSC-3	4	3.0	0.85	[95]
Fe-SA/PNC	4	3.2	0.83	[96]
FeAzPc-CNT	4	3.2	0.61	[97]
FeSNC-3	4	4.8	0.69	[98]
Fe-N-C	4	4.1	0.60	[99]
Fe@G-800/100	4	4.7	0.83	[100]
Fe0.05-N@MOF	4	6.6	0.56	[101]
Fe-N-C	4	5.4	0.77	[102]
Cu/NCNSs	2	1.8	0.77	[103]
Fe SAs/NC	4	4.8	0.75	[104]
Co−N/C fiber	4	2.2	0.74	[105]
Co/HNC	4	4.5	0.76	[106]
$MnFe_2O_4$/AC	4	5.0	0.60	[107]
FeCo-FePc/NTu-CNsh	4	4.8	0.82	[108]
FeNSC-ZM	4	6.1	0.66	[109]
FeN_4-Cu	4	5.2	0.81	[110]
Fe-NC(Zn^{2+})	4	5.6	0.61	[111]
FeMn PDA-900	2/4	3.9	0.71	[112]
Fe1/d-CN	4	5.6	0.61	[113]
FeRPM_BP	4	5.3	0.76	[114]
PT-MnN_4	4	3.1	0.63	[115]
FeCo-LT	4	5.0	0.83	[116]
FeCo-NC	4	5.2	0.81	[117]
Co-C	4	3.1	0.63	[118]
Ca_2FeRuO_6	4	5.0	0.78	[119]
CoNC@AC-850	4	4.1	0.34	[120]
P/Fe/N-SS	4	5.8	0.55	[121]
CuBPS	2/4	n.a.	0.50	[122]
Co/NCA	4	n.a.	0.70	[123]
Co-PB-1(6)	2	n.a.	0.63	[124]

(continued on next page)

Table 1 (*continued*)

Catalysts	n. electrons	Kinetic current density (mA cm^{-2}) @ 0.7 V vs. RHE	$E_{1/2}$ (V vs. RHE)	Ref.
IrP2@PC-0.96	4	n.a.	0.81	[125]
Fe/N/C-50	4	n.a.	0.81	[126]
Fe-N-C	4	4.8	0.82	[127]
Fe-N-C cig	4	3.3	0.43	[128]

synergistic interaction of transition metals (e.g., Fe, Cu, or Co) with nitrogen-doped carbon supports, which enhance active site exposure and facilitate efficient oxygen adsorption and reduction. FeCu/N-C (0.84 V), Fe-N-C (0.85 V), and FeCo-NC (0.81 V) exhibit the highest $E_{1/2}$ values, indicating superior ORR kinetics and lower overpotentials. These electrocatalysts benefit from highly active Fe-N_x coordination sites, which enhance charge transfer and oxygen binding. In contrast, electrocatalysts such as CoNC@AC-850 ($E_{1/2}$ = 0.34 V) and Cu-tmpa ($E_{1/2}$ = 0.31 V) exhibit significantly lower $E_{1/2}$ values, reflecting weaker electrocatalytic performance due to less effective active sites or suboptimal structural properties.

Fe/N/C-50, FeN_4-Cu, and FeCo-NC achieve balanced performance with high $E_{1/2}$ (0.81 V) and moderate to high kinetic currents (5.2–6.1 mA cm^{-2}), highlighting the effectiveness of doping strategies involving Fe and N coordination. Structural properties such as mesoporous frameworks and high BET surface areas contribute to enhanced mass transfer and active site utilization. Conversely, electrocatalysts like P/Fe/N-SS ($E_{1/2}$ = 0.55 V, kinetic current = 5.8 mA cm^{-2}) demonstrate high currents but lower $E_{1/2}$, suggesting trade-offs in activity optimization. Hence, electrocatalysts achieving the highest kinetic currents and $E_{1/2}$ values—such as FeCu/N-C, Fe-N-C, and Fe/N/C-50—illustrate the importance of synergistic effects between transition metals and nitrogen-doped carbon frameworks. These properties enable enhanced ORR activity by optimizing active site availability, charge transfer efficiency, and oxygen binding. Electrocatalysts with lower performance metrics tend to suffer from structural limitations such as low porosity, poor conductivity, or insufficient active site density, underscoring the importance of material design in maximizing ORR performance.

Despite the different ORR mechanisms and final products, carbonaceous-based electrocatalysts represent a valid alternative to metal-based and TNC. Notably, carbonaceous-based electrocatalysts are highly selective for H_2O_2 formation due to their low binding affinity for reaction intermediates and the retention of the O-O bond in alkaline media. Interestingly, some carbon-based electrocatalysts also display notable H_2O_2 selectivity in acidic and neutral environments. The adsorption of O_2 onto these electrocatalysts is hindered by a significant energy barrier, yet the reaction still favors H_2O_2 production, implying that the mechanism differs from the traditional adsorbed O_2 (O_2ads) pathway [129].

Chai et al. introduced the OOH^- ion mechanism, which describes how, in acidic conditions, hydrogenation of the electrocatalytic sites on carbon-based materials leads to the formation of specific hydrogen-active centers. These centers facilitate O_2 adsorption, forming OOH^-, which subsequently reacts with H^+ to generate H_2O_2. The process requires less energy for hydrogen extraction than for direct O_2 adsorption, making the $2e^-$ pathway more efficient at lower potentials in acidic environments [130].

As the pH increases, hydrogenation becomes less effective, and the O_2ads mechanism becomes more dominant, favoring the $4e^-$ ORR at higher potentials. Additionally, in a non-PCET mechanism, electrons and protons are transferred independently in a sequential manner. This pathway is characteristic of semiconductor electrocatalysts, where oxygen species (O_2^-(aq) or HO_2^-(aq)) first form through oxygen single-electron transfer (OSET) before being adsorbed onto the electrocatalytic sites. The uncoupling of proton and electron transfer in this mechanism leads to either H_2O_2 or HO_2^- formation, depending on the pH conditions [129].

Carbonaceous-based materials are promising electrocatalysts for H_2O_2 production due to their low cost, high electrical conductivity (10^3–10^4 S/m), and excellent chemical stability. While their performance in alkaline electrolytes (pH > 12) has been optimized, recent advancements have improved H_2O_2 selectivity in acidic media, though their activity in neutral pH conditions (pH ~7) is relatively low [131]. The introduction of oxygen functional groups (OFGs) has proven to enhance electrocatalytic efficiency, with oxidized carbon nanotubes (O-CNTs) achieving 90 % H_2O_2 selectivity in both alkaline and neutral media, though their E_{ONSET} in neutral conditions remains relatively low at 0.35 V vs. RHE [132]. Additionally, porous structure plays a crucial role in optimizing electrocatalytic performance by enhancing mass transport and active site accessibility. Microporous (micro C) and mesoporous (meso C) carbons, synthesized via polymerization and pyrolysis at 900 °C, exhibited H_2O_2 selectivity above 70 % in alkaline and neutral conditions, with meso C outperforming its microporous counterpart due to its larger average pore diameter (10–50 nm), which improved O_2 diffusion and mass transfer rates. The electrochemically active surface area (ECSA) of meso C (~800 m^2/g) was nearly double that of microporous carbon (~450 m^2/g), resulting in enhanced stability and prolonged electrocatalytic activity [26]. To further improve performance, mesoporous carbon hollow spheres (MCHS) were synthesized via a hard-template method, adjusting the precursor-to-template ratio to optimize pore size and oxygen content. These materials exhibited a specific surface area (SSA) of 900–1200 m^2/g, an oxygen content of 12–15 at%, and exceptional H_2O_2 selectivity of 99.9 % in 0.1 M phosphate-buffered solution (pH 8). Furthermore, their stability across potentials (0.35–0.62 V vs. RHE) remained above 90 % selectivity, making them highly effective electrocatalysts for on-site H_2O_2 production. Future research should focus on fine-tuning OFGs, optimizing pore connectivity, and enhancing long-term stability to further advance carbon-based electrocatalysts for scalable H_2O_2 electrosynthesis.

4. Enzyme-based electrocatalysts for ORR at neutral pH

The general ORR catalyzed by multi-copper oxidases (MCOs) begins with the single-electron oxidation of an electron donor (e.g., 2,2′-Azinobis(3-ethylbenzothiazoline-6-sulfonic acid)). This process is linked to the complete $4e^-$ reduction of O_2 to H_2O. The initial step involves ET electron transfer from the substrate to the T1 copper, which varies based on the MCO type, leading to the reduction of T1 copper [56]. Electrons then move internally to the trinuclear copper center (TNC) via a cysteine-histidine pathway spanning approximately 13 Å, reducing the copper ions in the TNC [133]. When four substrates are oxidized, all copper ions in the enzyme are fully reduced, as schematically depicted in Fig. 5A.

The MCOs electrocatalytic mechanism is reported in Fig. 5B. When the enzyme is fully reduced, it reacts with O_2 to form a peroxy intermediate (PI) [134,135]. This step depends linearly on oxygen concentration with a bimolecular rate constant of approximately 2 x 10^6 M^{-1} s^{-1} [134,136]. In the PI, both oxygen atoms exist as superoxide/peroxide species, bridging the T2 copper (in its oxidized state) and both copper atoms in T3 copper (one oxidized, one reduced) in a side-on bridged structure. The PI is then reduced to the native intermediate (NI) through reductive O-O bond cleavage, forming the T3 copper hydroxy bridge (T3μ_2OH bridge) [134,135,137]. This transition occurs via the PI + e^- intermediate state, where four electrons are transferred one by one from T1 copper and T2 copper before the O-O bond cleavage. The electron transfer between T1 copper and T2 copper is very rapid (k ~10^3 s^{-1}). The $2e^-$ reduction of PI to NI has a large thermodynamic driving force to overcome the Franck-Condon barrier for O-O bond cleavage. NI is the most oxidized state in the catalytic cycle and can be quickly reduced by an electron donor, returning to the fully reduced initial state for another cycle. Without an electron donor, NI slowly decays (k = 0.034 s^{-1}), releasing H_2O and transitioning to the

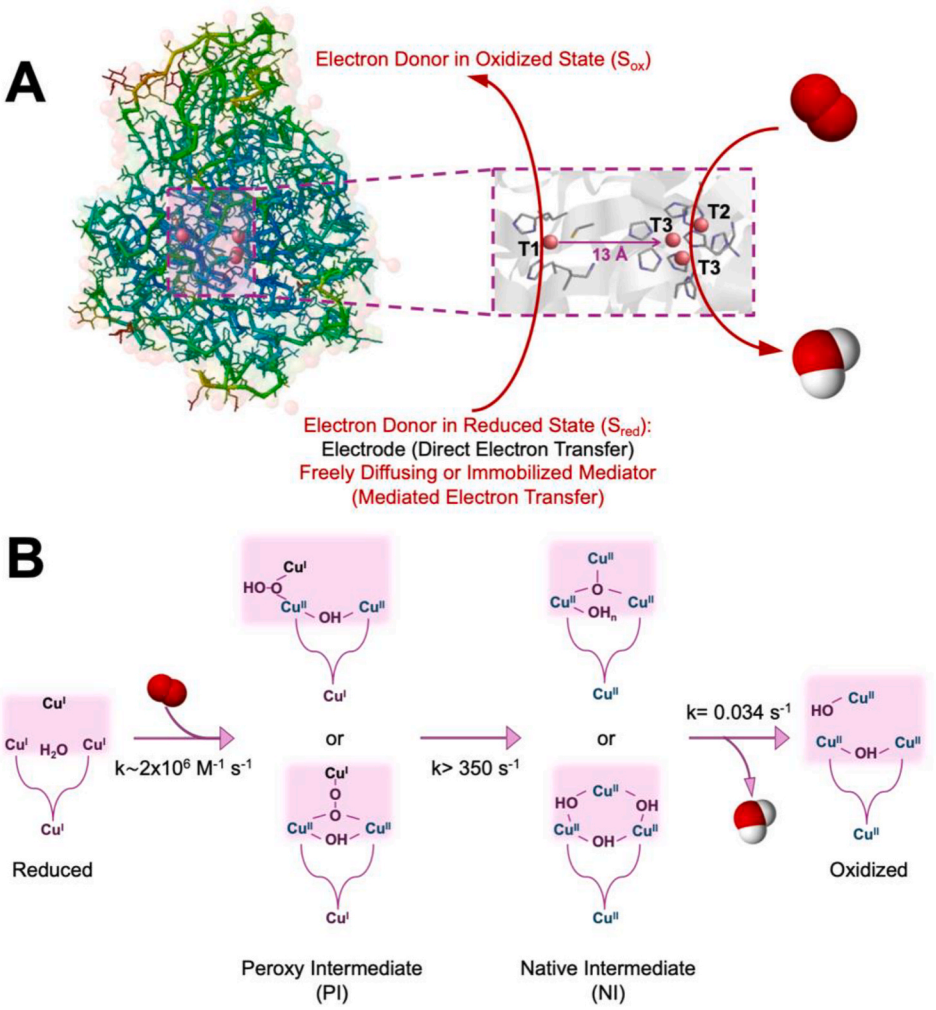

Fig. 5. **(A)** Scheme of electron transfer mechanism within MCOs during ORR. **(B)** Electrocatalytic pathway of ORR within MCOs from the fully reduced state through intermediate states (peroxy and native) towards resting oxidized state.

resting oxidized state with one oxygen atom from O_2 bound as OH to T2 copper [134]. The oxidized TNC in the resting oxidized state is further reduced to the fully reduced state. These steps via the resting oxidized state are too slow for the catalytic turnover mechanism [137,138]. Hence, the $4e^-$ reduction of O_2 to H_2O occurs in two $2e^-$ steps, with peroxide formation being the rate-limiting step, though the overall rate-limiting step in the enzyme-catalyzed ORR is considered the oxidation of the electron donor [136].

MCO-modified electrodes find wide applications in enzyme-based fuel cells (EFCs), biosensors, and pH-responsive biomolecule release electrodes. In EFCs, enzymes serve as electrocatalysts to produce electrical energy by oxidizing biomolecules like glucose at the anode and reducing O_2 at the cathode in biological environments [139]. However, EFCs currently operate at micro-scale power densities and face challenges in achieving efficiency and especially stability comparable to microbial fuel cells (MFCs) and non-biological fuel cells. Further investigation into bioelectrochemical processes is crucial for enhancing their performance.

Tang et al. investigated ORR catalyzed by bilirubin oxidase (MvBOD) immobilized on a 3D reduced graphene oxide (RGO)-modified carbon electrode [140]. To prevent RGO aggregation, 4-aminobenzoic acid (4-ABA) functionalization was employed, improving enzyme orientation and enabling direct electron transfer (DET) at neutral pH. Electrochemical analysis showed an electrocatalytic current density of 193 ± 4 $\mu A\ cm^{-2}$ in O_2-saturated PBS buffer (pH 7.0, 100 mM), with an E_{ONSET} of ~1.18 V vs. RHE and a half-life of 55 h, marking it as the most stable DET-type MvBOD biocathode to date. Integrating the bioelectrode into a gas-diffusion electrode (GDE) increased the electrocatalytic current density to 60 $\mu A\ cm^{-2}$ at 0.81 V vs. RHE, surpassing the submerged configuration (40 $\mu A\ cm^{-2}$). When applied in a membrane-less glucose/O_2 EFC, the system achieved a power density of 22 $\mu W\ cm^{-2}$ at 0.83 V and an open circuit voltage (OCV) of 1.12 V, demonstrating its viability for bioelectrochemical energy conversion.

Lipínska and co-workers reported the immobilization of MvBOD onto gold nanoparticles (AuNPs) supported by nanostructured titanium (Ti) surfaces [141]. The researchers varied the gold layer thickness (2 nm, 5 nm, 10 nm, 15 nm), resulting in AuNP sizes of 13 ± 6 nm, 46 ± 12 nm, and 81 ± 13 nm, to evaluate their impact on bioelectrocatalysis. Electrochemical characterizations demonstrated that MvBOD immobilized on 10 nm AuNPs (BOD-M-10Au@Ti) exhibited the highest catalytic performance, achieving a threefold increase in current density (1.2 ± 0.2 mA cm^{-2}) compared to bulk gold electrodes (0.4 ± 0.1 mA cm^{-2}). The ORR E_{ONSET} was measured at ~1.13 V vs. RHE, with optimal enzymatic activity at pH 6, where electrostatic interactions between MvBOD and self-assembled monolayer (SAM) on AuNPs were maximized. Long-term stability tests revealed that MvBOD on 10 nm AuNPs retained 100 % of its catalytic current over 10 h in 1 M Na_2SO_4, whereas bulk gold electrodes experienced a 40 % loss in activity over the same period. This suggests that the curvature of AuNPs enhances enzyme stability by reducing crowding effects.

Sedenho et al. immobilized MvBOD in a polymeric biogel matrix on a carbon-based GDE. The biogel, formulated with Nafion and crosslinked with glutaraldehyde, enhances enzyme stability and catalytic efficiency, supporting a DET-driven $4e^-$ ORR pathway [142]. Electrochemical assessments revealed a maximum catalytic current density of -1.5 ± 0.2 mA cm^{-2} at 0.80 V vs. RHE, with an E_{ONSET} of ~1.16 V vs. RHE. The process exhibited a $4e^-$ reduction of O_2 to H_2O. The biogel thickness (~2.1 ± 0.2 μm) was optimized to prevent enzyme loss while ensuring high catalytic activity. Durability tests indicated that the bioelectrode retained ~97 % of its initial current density after 24 h at a steady current of -1.00 mA cm^{-2}, and maintained stable ORR potential (~1.16 V vs. RHE) even after open-circuit storage. These results demonstrate that the BOD-based biogel provides a highly stable and efficient solution for enzymatic air-breathing cathodes, offering potential applications in biofuel cells and bioreactors where enzyme longevity and performance are critical.

Torrinha et al. developed a bioelectrode incorporating MvBOD into a nanostructured carbon paper (CPA) transducer, highlighting its effectiveness for microenergy generation in biobatteries and dioxygen sensing [143]. When integrated into a zinc-BOD biobattery, the system delivered an OCV of 1.69 V and reached a maximum power density of 165 μW cm^{-2}, with a short-circuit current density of 94 μA cm^{-2}. The electrochemical analysis confirmed a high ORR E_{ONSET} of 1.17 V vs. RHE at pH 7.1, demonstrating efficient electron transfer. The bioelectrode exhibited excellent operational stability, retaining 88 % of its initial activity after 34 days, attributed to the strong enzyme attachment via 1-pyrenebutanoic acid N-hydroxysuccinimide ester (PBSE). As an O_2 biosensor, the MvBOD-modified electrode showed a sensitivity of 606 ± 22 μA mM^{-1} cm^{-2} at 1.01 V vs. RHE and a limit of detection (LOD) of 1.3 ± 0.2 μM, while maintaining selectivity against potential interfering compounds such as glucose, citric acid, and sodium chloride.

Carrière et al. reported on MvBOD immobilized onto MWCNTs modified with glyconanoparticles (GNPs), aiming to enhance DET and catalytic performance [144]. GNPs functionalized with anthraquinone sulfonate (AQS), establish a negatively charged interface that facilitates enzyme orientation and boosts electron transfer efficiency at the electrode surface. Electrochemical evaluations showed an ORR E_{ONSET} of 1.11 V vs. RHE, with a peak cathodic current density of -0.88 mA cm^{-2} at 0.81 V vs. RHE, significantly surpassing control electrodes modified solely with MWCNTs (-0.07 mA cm^{-2}) or unmodified GNPs (-0.05 mA cm^{-2}). The enzyme-electrode interaction was characterized by an AQS surface coverage of 8.0×10^{-9} mol cm^{-2}, corresponding to 48–72 monolayers, ensuring effective DET. Stability tests indicated that the bioelectrode retained 88 % of its initial current density after 50 consecutive scan cycles, highlighting strong enzyme adherence and minimal degradation.

Xiao et al. reported an innovative approach to enhancing ORR by incorporating polytetrafluoroethylene (PTFE) submicro-rods as localized "oxygen tanks" within MvBOD-modified cathodes. Electrochemical analysis revealed a formal redox potential ($E^{0'}$) of 0.68 V vs. RHE and an ORR E_{ONSET} of 0.91 V vs. RHE [145]. The optimized configuration, where PTFE was mixed directly within the redox polymer matrix, achieved a maximum cathodic current density of 36.6 ± 2.2 μA cm^{-2} at 0.68 V vs. RHE, outperforming the PTFE-free counterpart by 17 %. More importantly, this configuration significantly improved the operational stability, maintaining 84 % of its initial current density after 16 h, whereas the PTFE-free electrode lost nearly all activity within 7 h.

Nishida et al. examined MvBOD structure, which has two N-linked glycan binding sites, N472 and N482, and applied site-directed mutagenesis along with polyethylene glycol (PEG) modifications to assess their influence on enzyme orientation and electron transfer [146]. Electrochemical measurements identified a formal redox potential ($E^{0'}$) of 0.45 V vs. RHE and an ORR E_{ONSET} of 0.50 V vs. RHE for both the unmodified and modified enzymes. The maximum cathodic current density (J_{max}) for the native enzyme (eBOD) was -4.0 ± 1.0 mA cm^{-2}, while modification at the N472 site (N472C-PEG12-eBOD) led to a significant decline in performance, reducing J_{max} to -0.7 ± 0.2 mA cm^{-2}, an 82.5 % decrease, likely due to steric interference near the T1 Cu active site (21.9 Å). In contrast, altering the N482 site (N482C-PEG12-eBOD) had a minor effect, retaining 75 % of the DET activity with a J_{max} of -3.0 ± 0.3 mA cm^{-2}, suggesting that its greater distance from the active site (35.7 Å) makes it less disruptive. Additionally, incorporating an acidic functional group (N472C-PEG12-acid-eBOD) slightly improved enzyme orientation due to electrostatic repulsion but still experienced steric hindrance, resulting in a J_{max} of -1.0 ± 0.2 mA cm^{-2}. These results demonstrate that glycan structures play a vital role in controlling DET efficiency and indicate that optimizing glycan composition could enhance BOD-based bioelectrodes for improved biofuel cells and biosensors.

Interestingly, BES composed of microbial biocatalyst at the anode electrode combined with enzymatic biocatalyst ORR at the cathode electrode were presented. Cooney et al. showed firstly this hybrid BES with *Shewanella* bacterial anode and laccase cathode [147]. The two compartments were divided by a polymeric membrane achieving an OCV of over 1 V and a 5th day stable performance under galvanic polarization. Santoro et al. introduced bilirubin oxidase at the cathode while the anode was colonized by a mixed bacterial culture [148]. The hybrid MFC was able to achieve as high as 200 μW cm^{-2} with cathode OCP recording above 1.1 V vs RHE. The durability of BOx enzymatic air-breathing cathode was also recorded for over 45 days of operation in neutral media (phosphate buffer) under pristine and polluted environments [149]. In a clean environment, simply using PBS, the OCP remained stable while the limiting current decreased. In polluted environments instead, the OCP decreased as well as the limiting current.

Moreover, ORR in neutral media represents one of the most studied electrochemical processes used to accomplish the local pH change at the electrode/solution interface [150–152]. This process can take place through different mechanisms mostly depending on the electrode material, applied potential, current density, and the used electrocatalysts.

In particular, self-powered drug delivery systems based on conductive polymers (CPs) were developed, utilizing osmium redox polymer-mediated glucose/O_2 EFCs with an additional CP-drug layer on the cathode (Fig. 6A–D) [153]. Controlled release of model drug compounds like ibuprofen, fluorescein, and DAPI was achieved upon discharge in the presence of glucose and oxygen, demonstrating applicability for implantable devices (Fig. 6E, F and **G**). Alternatively, the ORR operated from MCOs can yield to local (interfacial) pH increase due to the consumption of H^+ ions required for the formation of H_2O [154]. To realize a pH-switchable (bio)molecule release electrode, ORR catalyzed by MCOs should be combined with a pH-sensitive electrode surface like trigonelline/boronic acid composite [156,157]. Thus, the local pH change results in the production of the negative charge at the interface and the repulsion/release of the electrostatically loaded DNA [158]. In this application, the main drawback is the re-equilibration of interfacial pH change due to the high buffer capacity of bulk solution (Fig. 6H) [159].

Local pH changes reverse the charge of SiO_2 nanoparticles (200 nm, modified with pH-sensitive polymers), releasing DNA molecules as the surface shifts from positive to negative during ORR [156]. BOD bioelectrocatalytic activity generates a mild electrical potential for ORR, applicable through *in situ* biocatalytic or photo-biocatalytic processes [156,157]. This method offers a versatile platform for the precise release of biomolecules and nanomaterials triggered by various signals. Recently, Tricase et al. introduced a method to regulate semiconductor nanoparticle synthesis using a bionanoreactor driven by (bio)electrochemical stimuli, specifically pH changes induced by ORR (Fig. 6I, J and **K**) [155]. Bioelectrochemical synthesis yielded CdSe NPs with an average diameter of 4 ± 1 nm after 90 min of voltage application in the presence of O_2, showing promise for nanoparticle synthesis in biological media despite challenges in optimizing the process.

Similarly, artificial enzymes designed for ORR leverage principles of supramolecular catalysis to mimic the efficiency and selectivity of

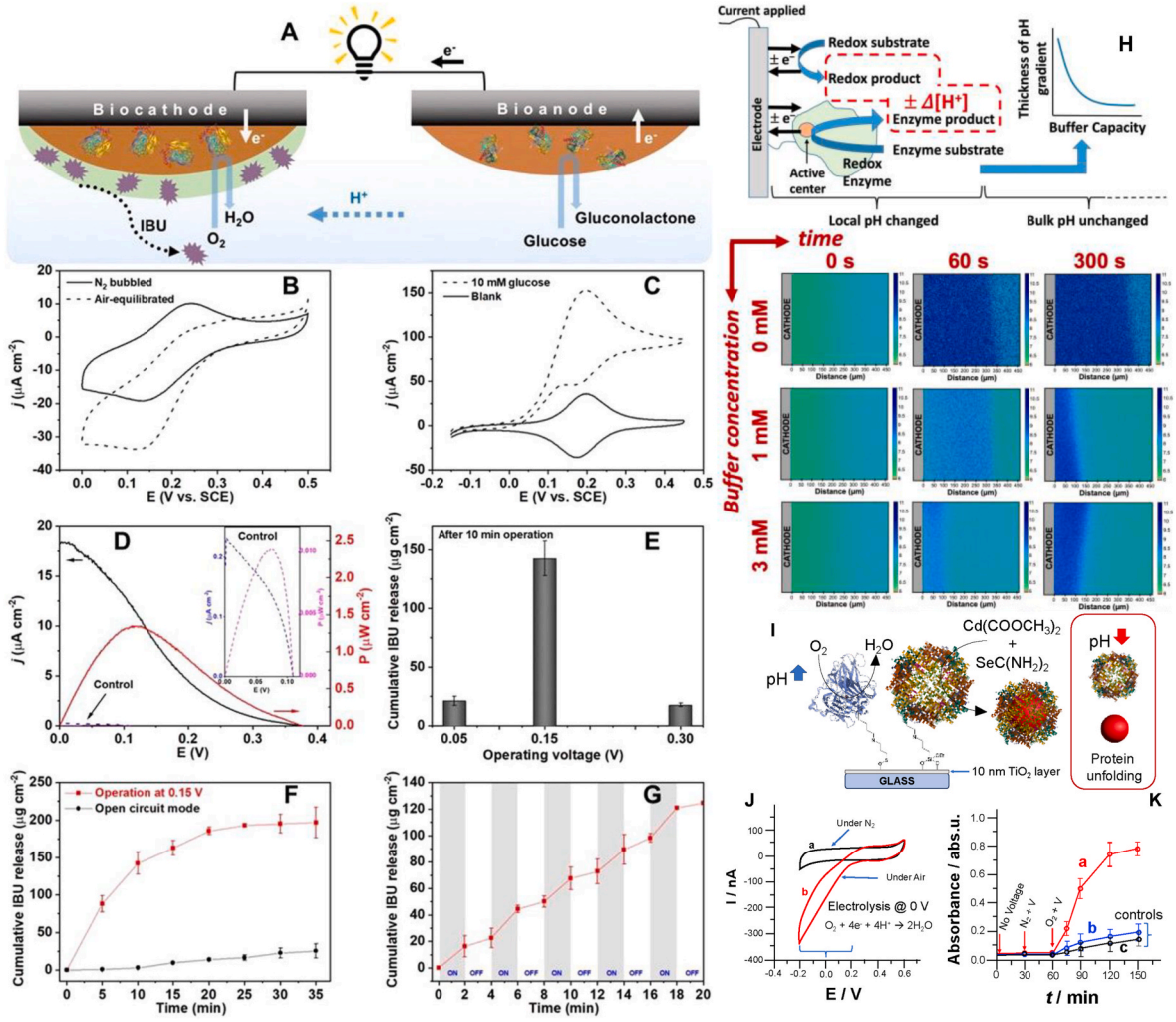

Fig. 6. **(A)** Diagram showing the regulated release of IBU using an EFC. (CVs for the IBU loaded nanoporous gold electrode **(B)** and nanoporous GOx-modified electrode **(C)** in phosphate buffer. **(D)** Polarization curves for EFC, which includes the GOx-modified bioanode and the IBU-loaded biocathode, with 10 mM glucose and without as control experiment (Inset in **D**). **(E)** Total IBU released from the EFC at different voltages. **(F)** IBU release profile at 0.15 V (red curve) and at open-circuit voltage (black curve). **(G)** Total IBU released in ON-OFF mode (alternating between 0.15 V and open circuit voltage). **(H)** Local pH change occurring at MCOs modified electrode where the thickness of the layer is correlated with buffer concentration and time. **(I)** Diagram of a Ti electrode modified with laccase/apoferritin for pH-triggered synthesis and release of CdSe nanoparticles due to ORR. **(J)** CVs of Ti-modified electrode with ferritin and laccase in the absence and precence of O_2. **(K)** UV–Vis kinetics at 0 V vs. Ag/AgCl: (a) CdSe NP synthesis by ORR-catalyzed pH change, (b) control without laccase at 0 V, (c) control without voltage. Panels A–G were adopted with permission of American Chemical Society from Ref. [153], Copyright 2020. Panel H was adopted with permission of Wiley from Ref. [154], Copyright 2021. Panels I–K were reproduced with permission of Royal Society of Chemistry from Ref. [155], Copyright 2024 under CC-BY-3.0 http://creativecommons.org/licenses/by/3.0/. (For interpretation of the references to colour in this figure legend, the reader is referred to the Web version of this article.)

natural metalloenzymes [160]. These synthetic systems often incorporate transition metal complexes, macrocyclic ligands, and cooperative multi-metallic centers to facilitate oxygen activation and electron transfer. Unlike traditional catalysts, artificial enzymes are engineered to replicate key structural and functional features of biological electrocatalysts, such as active site architecture, substrate recognition, and cofactor coordination. By fine-tuning ligand environments and incorporating secondary coordination interactions, these mimetic systems enhance O_2 binding, activation, and selective reduction to either H_2O_2 ($2e^-$ pathway) or H_2O ($4e^-$ pathway) [161].

A key biological example is the heme-copper binuclear center (BNC) in cytochrome *c* oxidase (CcO), responsible for reducing over 90 % of O_2 to H_2O in living organisms. In CcO, the released energy powers proton translocation across the mitochondrial membrane, driving ATP synthesis. Structurally, the BNC consists of high-spin Fe^{II} (heme a_3) and Cu^{I} (CuB), which synergistically facilitate O_2 binding, activation, and reduction [162].

The electrocatalytic mechanism comprises oxidative and reductive phases. Initially, O_2 binds to FeII, forming a superoxide intermediate, followed by homolytic O–O bond cleavage, producing Fe^{IV}=O (ferryl) and Cu^{II}-OH species. The rapid $4e^-$ transfer prevents the accumulation of peroxo intermediates, enhancing efficiency. In the reductive phase, four protons and three electrons restore the enzyme to its reduced R state, coupling proton uptake with membrane transport. The CuB center plays a critical role in O–O bond cleavage, distinguishing this system from cytochrome P450, where heterolytic scission occurs. The heme-copper active site serves as a model for designing synthetic bio-inspired ORR electrocatalysts with enhanced efficiency and selectivity.

Notably, PCET plays a crucial role in directing the reaction pathway and determining product selectivity. Tse et al. proposed a Cu-based complex (CuBTT) as an artificial enzyme incorporated into a hybrid bilayer membrane (HBM) to regulate proton transport precisely [46]. This system consists of a SAM of CuBTT chemically attached to a gold electrode, with a lipid monolayer containing 1-dodecylboronic acid

(DBA) as a proton transfer mediator. The presence of DBA-modulated proton flux favors the four-electron reduction of O_2 to H_2O while minimizing the production of undesirable intermediates such as H_2O_2 and O_2^-. In the absence of a lipid monolayer, CuBTT facilitated a mixed $2e^-$ and $4e^-$ ORR, yielding approximately 0.11 mol of H_2O_2 per mole of O_2 consumed. However, in the presence of a lipid layer without a proton carrier, H_2O_2 formation increased to 0.68 mol per mole of O_2, indicating a shift toward the two-electron pathway due to restricted proton availability. The introduction of 10 mol% DBA within the lipid monolayer completely redirected the reaction towards $4e^-$ pathway, eliminating H_2O_2 formation.

The reaction mechanism follows a PCET process, where the rate of proton movement determines whether the ORR proceeds via $1e^-$, $2e^-$, or $4e^-$ pathways. Effective coordination between proton transport, electron transfer, and O–O bond cleavage is critical for ensuring selective O_2 conversion to H_2O. By optimizing proton flux, the CuBTT-based system exhibited enhanced ORR efficiency and selectivity, highlighting the importance of proton transport regulation in improving electrocatalytic performance for fuel cell applications.

The electrocatalysts listed in Table 2 exhibit a wide range of E_{ONSET} and current output densities at 0.8 V vs. RHE, with notable differences in stability. The highest onset potential is observed for MgOC ink-CMC/MvBOD (1.20 V vs. RHE), followed closely by MvBOD-based biogel/C GDE and CP/MWCNT/PBSE/MvDOB (1.19 V vs. RHE), whereas the lowest E_{ONSET} is recorded for Mg-N-C (0.83 V vs. RHE). In terms of current density at 0.8 V vs. RHE, Mg-N-C (4.50 mA cm^{-2}) and PG/MvBOD (5.10 mA cm^{-2}) stand out with the highest values, significantly outperforming MvBOD-M-10Au@Ti (0.02 mA cm^{-2}) and $Os(bpy)_2$PVI-BOx-PTFE(2)/GCE (0.04 mA cm^{-2}), which exhibit the lowest performance. Stability trends vary, with eBOD/ABA/KB/GCE and MWCNT/GNPPSCD/AQS/MvBOD maintaining 88 % of their initial current densities after 50 cycles, while 6A2NA–MvBO-modified PGE lost 50 % of its activity in just 6 h. The MvBOD-based biogel/C GDE and $Os(bpy)_2$PVI-BOx-PTFE(2)/GCE electrodes retained 84 % of their initial current densities over 24 and 16 h, respectively, indicating relatively good durability. These variations highlight the influence of different electrode compositions on electrochemical performance, with Mg-N-C and PG/MvBOD emerging as the most promising electrocatalysts in terms of current output, whereas MgOC ink-CMC/MvBOD demonstrates the highest E_{ONSET}.

Enzyme-based electrocatalysts offer high onset potentials and selectivity but suffer from lower stability. Artificial enzyme-based electrocatalysts, especially those utilizing nanomaterials like Mg-N-C, can achieve comparable or even superior current densities while providing enhanced stability. However, some artificial electrocatalysts still lag E_{ONSET}, requiring further optimization to match the oxygen affinity and active-site efficiency of natural enzymes.

Table 2
Comparison between enzyme-based and artificial enzyme-based electrode for ORR at neutral pH (*representative papers within last 5 years*). Abbreviations: 6A2NA-MvBO (MvBOD immobilized onto 6A2NA), ABA (4-aminobenzoic acid), AQS (anthraquinone-2-sulfonic acid), BP (buckypaper), CMC (carboxymethyl cellulose), CP (carbon paper), GCE (glassy carbon electrode), GDE (gas diffusion electrode), KB (ketjenblack carbon), eBOD (*escherichia coli* bilirubin oxidase), MgOC (magnesium oxide-carbon composite), MvBOD (*Myrothecium verrucaria* bilirubin oxidase), MWCNT (multi-walled carbon nanotubes), $Os(bpy)_2$ (osmium redox polymer), PGE (pencil graphite electrode), PBSE (1-pyrenebutyric acid N-hydroxysuccinimide ester), PG (porous gold), PTFE (polytetrafluoroethylene), PVI (polyvinylimidazole), Py (pyridine), rGO (reduced graphene oxide).

Catalysts	E_{ONSET} (V vs. RHE)	Current Output Density (mA cm^{-2}) @ 0.8 V vs. RHE	Stability	Ref.
MvBOD-M-10Au@Ti	1.13	0.02	n.a.	[141]
eBOD/4-ABA/KB/GCE	1.11	4.00	88 % of its initial current density after 50 continuous scan cycles	[146]
BP/4-ABA/MvBOD	1.02	1.20	n.a.	[163]
MWCNT/GNPPSCD/AQS/MvBOD	1.11	0.88	88 % of its initial current density after 50 continuous scan cycles	[144]
CP/MWCNT/PBSE/MvDOB	1.19	0.17	88 % of its response after 34 days	[143]
MgOC ink-CMC/MvBOD	1.2	1.40	n.a.	[164]
MvBOD-based biogel/C GDE	1.19	1.52	84 % retention of initial current density after 24 h	[142]
$Os(bpy)_2$PVI-MvDOD-PTFE (2)/GCE	1.02	0.04	84 % retention of initial current density after 16 h	[145]
MvBOD/4-ABA/rGO GDE	1.12	0.06	half-lifetime stability of 55 h	[140]
PG/MvBOD	1.19	5.10	n.a.	[165]
MWCNT/Py MvBOD	1.15	2.43	n.a.	[166]
Mg-N-C	0.83	4.50	85 % of normalized current after 10 h	[167]
6A2NA–MvBO-modified PGE	0.85	0.70	50 % activity was lost in 6 h	[168]

5. Microbial-based electrocatalysts for ORR at neutral pH

Electroactive microbial biofilms have been investigated since the 1980s for their ability to use electrodes as electron donors (microbial cathodes or biocathodes) and catalyze ORR. Initially studied in relation to metal aerobic biocorrosion, they gained attention in MFC applications from the beginning of the years 2000 onwards [169–171]. These biofilms develop naturally on artificial electrodes and conductive natural solid materials, but their controlled growth is limited or absent and it poses challenges due to the absence of precise tools or methodologies to take control and drive their growth and structural organization on the electrodes. In fact, a wide range of biotic and abiotic factors impact the growth and electrocatalytic performance of these electroactive biofilms (EAB) both on the anode for the oxidation reaction and on the cathode for the reduction reaction [172].

From a mechanistic point of view, key enzymes involved in direct microbial ORR include superoxide dismutases, catalases, and peroxidases, which protect microbes from oxidative stress and catalyze ORR when attached to surfaces [173]. Studies have shown that prosthetic groups of these enzymes, like iron porphyrins, adhered to surfaces, can catalyze ORR [174]. These compounds, along with organometallic compounds formed by metallic cations with extracellular polymeric substances (EPS) and flavins secreted by bacteria, act as ORR electrocatalysts. However, inhibitors of enzyme activity reduce ORR electrocatalysis, suggesting that active enzymes are crucial. Recently, a fascinating but unconfirmed ORR pathway involves direct electron transfer from the cathode to the microbial cell, which uses these electrons for respiration and releases them to oxygen [57,175].

Some bacteria in environments containing manganese or iron ions oxidize these metallic ions to oxides such as manganese oxyhydroxide (MnOOH), facilitating ET to oxygen for bacterial energy use [176–178]. This process, studied with manganese and bacteria *like Leptothrix discophora*, explains the fundamentals of the initiation of metal aerobic biocorrosion, also known as aerobic microbiologically influenced corrosion (MIC) and has been replicated in lab settings with pure cultures [179,180].

In general terms, MFCs are promising for generating low-cost electricity from sustainable organic compounds. Typically, in the majority of works in the literature, MFCs have an anaerobic microbial anode and a

non-biological, abiotic, inorganic ORR cathode [181]. However, the efficiency of these abiotic air cathodes is very often limiting at the neutral pH, operating conditions required for microbial anodes, posing a significant challenge for scaling up this type of BES [182,183]. Currently, MFCs with non-biological ORR cathodes achieve a power density of about 7 W m^{-2} (~50 A m^{-3}) in small-scale cells (~1 L volume), but this efficiency drops significantly in larger systems, especially with large-size electrodes [184].

Using ORR microbial cathodes can be an efficient alternative to abiotic ORR cathodes [185]. However, pairing microbial anodes with microbial cathodes creates a pH gradient due to proton production at the anode and hydroxide production at the cathode [186]. Particularly, local pH change at the bioanode hinders microbial growth and reduces biofilm electrocatalytic activity, while increasing pH at the biocathode reduces ORR efficiency by slowing reaction kinetics, particularly for catalysts suited to near-neutral conditions. Additionally, high alkalinity causes Ca^{2+} and Mg^{2+} to precipitate, forming carbonate and hydroxide deposits that degrade cathode performance [187–190]. Chemical buffers can address proton transport deficiencies but are costly and hard to manage for large-scale use [191–193]. A loop configuration, directing anode effluent to the cathode, reduces the pH gradient and enhances cathode performance but requires careful operation to avoid issues with oxygen supply and consumes extra energy to power the effluent circulation pumps [194]. Reversible bioelectrodes can solve the pH gradient problem and improve oxygen reduction by using biofilms to catalyze both anodic and cathodic reactions in successive or alternative time phases [195,196]. This method avoids strict aerobic bacteria growth and leverages proton accumulation during the anodic phase to boost the cathodic reaction. Systems using reversible electrodes, such as solar-powered MFCs and dual bioelectrode MFCs with polarity reversal, show significant power density improvements [197]. Despite their promising advantages, reversible microbial electrodes are not well-studied, and the microbial composition and long-term evolution of these biofilms remain largely unexplored [176].

The electrode material widely used to design bacterial ORR cathodes is carbonaceous-based such as graphite, in the form of monolithic materials or granular and filamentary materials [198,199]. Carbon surfaces that are extremely hydrophobic limit the formation of aerobic electroactive biofilms in three-dimensional electrode geometries, especially in the core of the porosity where water has difficulty accessing. However, surface structuration of carbon materials to create micrometer-scale roughness or the deposition of thin layers of hydrophilic polymers can reduce the hydrophobicity of the surfaces and promote the development of bacterial biofilms [200–203]. Strycharz-Glaven et al. explored microbial oxygen reduction at the biocathode of a sediment/seawater-based microbial solar cell (MSC), demonstrating that its catalytic activity does not rely on light [204]. Notably, the dark-incubated biocathode produced higher current densities than the illuminated one. CVs revealed a sigmoidal current-potential relationship, indicating heterogeneous electron transfer facilitated by an immobilized redox cofactor. Microbial community analysis showed that the biocathode biofilm in the dark-grown MSC was predominantly composed of *Marinobacter* spp. within the Gammaproteobacteria class, forming a multi-layered biofilm up to 8.2 μm thick. Even after repeated medium replacements, the biofilm retained its catalytic function and could sustain growth using inorganic carbon as its sole carbon source. In a three-electrode system, the enriched biocathode exhibited a maximum current density between −0.035 and −0.045 A m^{-2}, with a midpoint potential of approximately 0.475 V vs. RHE. Less widespread, stainless steel (SS) has shown a duality of behavior as a function of the salinity of the electrolytic solution and the grade of SS alloy used [205]. Strong SS alloys (316L, 254SMO) can outperform the performance of carbonaceous materials in a marine environment as they are more tolerant to high salt concentrations and less prone to corrosion [206].

Abiotic ORR occurring directly on the surface of metal-based, TM-N-C and carbonaceous electrode material can lead to the production of intermediates and several ROS species like H_2O_2, O_2^- and *OH triggering both Haber-Weiss and Fenton reactions in the presence of iron [174,207]. Indeed, Indeed, reactive oxygen species (ROS) exert a dual effect on bacterial biofilms. They induce cellular and DNA damage, leading to mutations, structural alterations, and potential cell death. However, ROS can also stimulate biofilm formation as a protective response, enhancing bacterial resilience. This complex interaction plays a crucial role in biofilm dynamics and antimicrobial agents resistance [208]. Alkalization at the cathodic surface by the production of hydroxyl ions (product of the ORR at neutral pH) results in the precipitation of hydroxides that precipitate in the biofilm or deposited on the electrode surface, causing fouling on the cathode surface [209–211].

Different strategies affect the efficiency of microbial biocathodes in ORR. Marine biofilms on stainless steel electrodes show similar ORR activity regardless of the potential applied during biofilm formation or growth on the electrode. In contrast, the growth of cathodic biofilms from aerated sludge collected in wastewater treatment plants revealed significant potential-dependent variations in microbial composition and ORR performance [212]. Microbial oxygen-reducing biofilms (EABs) cultivated on graphite rods were analyzed under both anoxic and oxygenated conditions. The cathodic current density stabilized at approximately -71 ± 6 μA cm^{-2} at 0.821 V vs. RHE, with an $E_{1/2}$ recorded at 0.972 V vs. RHE at pH 7.8. When exposed to air, CVs exhibited a sigmoidal shape, indicating quasi-reversible heterogeneous electron transfer (HET) for O_2 reduction. The biofilms efficiently catalyzed the complete reduction of O_2 to H_2O through a $4e^-$ pathway, with an E_{ONSET} for O_2 reduction observed at 1.091 V vs. RHE. The redox properties of the biofilm varied with pH, showing significant changes between pH 6 and 9.5, while activity drastically declined below pH 5, disrupting the characteristic sigmoidal polarization curve [213].

The design of microbial biocathodes is essentially used as inoculum complex industrial or environmental, chemically variable media such as wastewater, seawater or marine sediments and soils. Extracts and leachates from these media lead to the selection of even more electroactive bacterial populations [196,214].

In MFC research, key metrics like power and current generation, chemical oxygen demand (COD) removal, and coulombic efficiency (CE) are commonly reported. COD removal and CE are straightforward to measure, especially with known substrates like acetate. Reporting current and power involves different normalization methods, which vary by electrode surface area, electrode volume, or MFC compartment volume. Studies highlight both regional similarities and differences, complicating the identification of individual parameter impacts due to numerous variables.

Larrosa et al. emphasized the need for more replicates in MFC tests due to low repeatability. Mateo et al. found that running over 100 MFCs simultaneously under the same conditions could reduce uncertainty in the maximum current probability to less than 5 % [215,216].

To develop simple and reproducible methods, five institutions from the US and Europe conducted a cross-laboratory study, strictly following a standardized protocol. They examined the influence of local domestic wastewater's microbial composition on MFC performance, including voltage, power, current production, COD removal, pH, and microbial population dynamics. Hence, it is not trivial to grow microbial populations around the world, as shown in Fig. 7A–E (electrochemical and microbiological cross-laboratory study) [217].

The statistical analysis revealed that the bacterial communities on the cathodes were like those in the effluent, whereas the anodic biofilms varied significantly between institutions and were closely related to the source of the inoculum. Importantly, even anaerobic bacteria were found on the cathode indicating probably a structure in layers of the biofilm forming on the cathode. In fact, it was speculated that aerobic bacteria stand on the part close to the air consuming the oxygen from penetrating to the anode chamber while strictly anaerobes were in the more internal part, protected by eventual air presence.

Only a few authors describe aerobic bacterial cathodes operating

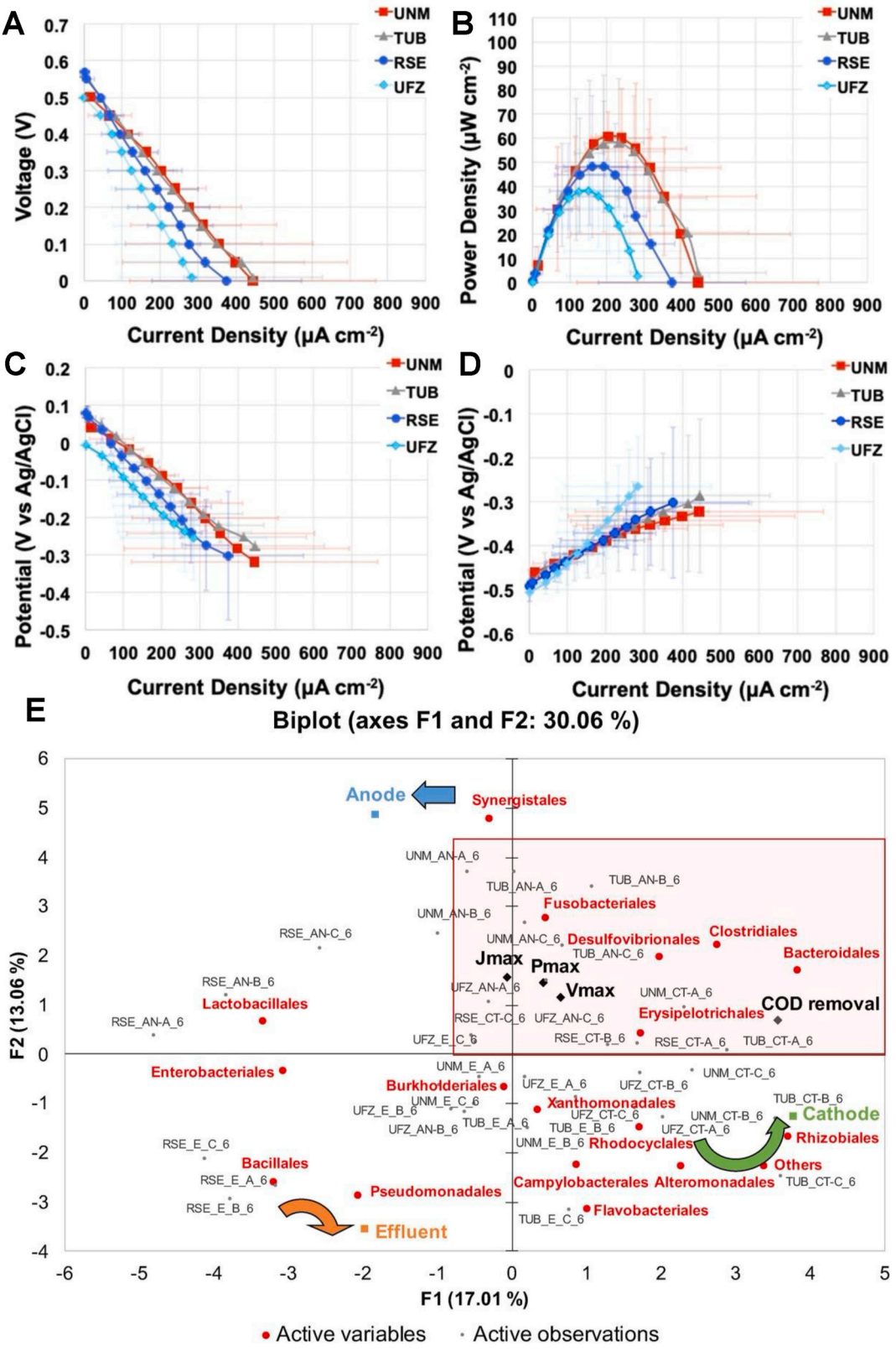

Fig. 7. MFC polarization **(A)** and power curves **(B)** and cathode **(C)** and anode **(D)** polarization curves carried out during cycle 6. **(E)** PCA biplot for all tested electrodes. Adopted with permission of Wiley from Ref. [217], Copyright 2021 under CC BY-4.0 https://creativecommons.org/licenses/by/4.0/.

from pure bacterial cultures [218,219]. Electroautotrophic bacterial communities are apparently much more robust than monocultures since some members are not grown individually outside the electrode environment at all, and electrochemical performance is more restricted in pure culture [220]. Yates et al. reported that *Marinobacter-Chromatiaceae-Labrenzia* (MCL) biofilm functions as an electroautotrophic microbial system capable of reducing oxygen at neutral pH by directly acquiring electrons from an electrode [221]. Operating at

0.51 V vs. RHE, the biofilm facilitates oxygen reduction without relying on hydrogen as an intermediary. Measurements using electrochemical gating reveal that long-distance extracellular electron transport (LD-EET) extends at least 5 μm beyond the electrode surface, allowing cells beyond direct contact with the electrode to participate in electron uptake. The biofilm exhibits electrical conductivity of 60 μS/cm at 30 °C, which is more than ten times higher than previously reported values for microbial biofilms, demonstrating its exceptional electron transport capabilities. Spectroscopic analysis, including confocal resonance Raman microscopy, has identified c-type cytochromes as the key redox mediators involved in this process. Environmental aerobic biofilms contain microbial populations with strong syntrophic relationships. The cultivable fraction of these biofilms is generally less than 1 x 10^{-2} %, demonstrating that most microbial species have a vital need to live in the community. Finally, pure cultures have a shorter operating time than those grown in mixed culture and they are prone to possible contamination that might affect their purity and cell density at the scale of the cathode surface area [222].

6. Cathode upscaling for improved renewable energy production

In the sections above, ORR mechanisms, limiting steps, and negative effectors occurring over biotic/abiotic at the active site level have been discussed in detail. To operate, these electrocatalysts need to be integrated into cathode electrodes and their architecture optimization is considered and discussed in this section. Integrating the electrocatalyst into the cathode architecture posed numerous challenges related to transport phenomena, current distribution and the effects of chemical and physical processes spanning scales from angstroms/nanometers to millimeters [223,224].

Two main cathode configurations are used in BESs which might incorporate: i) cathode fully immersed into an aqueous solution; ii) cathode open to the air (known as a gas diffusing electrode, GDE), Fig. 8) [171]. The first configuration operates with the cathode electrode fully submerged within a liquid-phase electrolyte. The major characteristic of this cathode is the fact that being completely in contact with the liquid, the surface must be hydrophilic to enhance the contact of the electrocatalytic sites with the electrolyte [225]. The reaction occurs at a two-phase interface (liquid and solid) and oxygen as a reagent is dissolved into the liquid phase. Indeed, the protons and the reactants are soluble in the liquid phase, while the electrocatalytic sites on the cathode are in a solid phase. Therefore, the utilization of hydrophilic binder is preferred to enhance the electrocatalyst/electrolyte interaction/affinity for maximizing the surface of the liquid/solid interface and oxygen in dissolved form. Particularly, dissolved O_2 is needed for bacterial ORR [226].

Dissolved O_2 is strictly dependent on the air pressure, the salinity of the electrolyte and the temperature with the latter being regulated by Henry's law [227]. Dissolved O_2 decreases with the increase in salinity content and temperature and lower air pressure. For example, at sea level, at 25 °C and with electrolyte salinity of 1 g L^{-1} (referred to as total salt content), dissolved oxygen is ≈ 8 mg L^{-1} (0.24 mM). The oxygen concentration in air is roughly 21 % which corresponds to a molar concentration of 8.6 mM which is roughly 35 times larger compared to dissolved O_2.

Since the ORR frequently limits the performance of BESs, a higher concentration of reactant is required. As a result, atmospheric oxygen is preferred and more efficient than dissolved O_2 in the electrolyte [170]. Operation with passive mass transfer based on simple diffusion phenomenon is also preferred. The open-to-air cathode-type does not need oxygen to be provided through the external utilization of energy-consuming pumps, but its own architecture is built to provide passively the reactant. Particularly, air-breathing cathodes are specifically designed in two main layers or zones [147,228]. The first one facing the electrolyte has mainly hydrophilic or slightly hydrophobic characteristics. The second one, contiguous to the first one, has mainly hydrophobic characteristics. The second region/zone usually ends on the current collector or with the diffusion layer, reasonably closer to the atmosphere. Each of these two regions has a particular function to

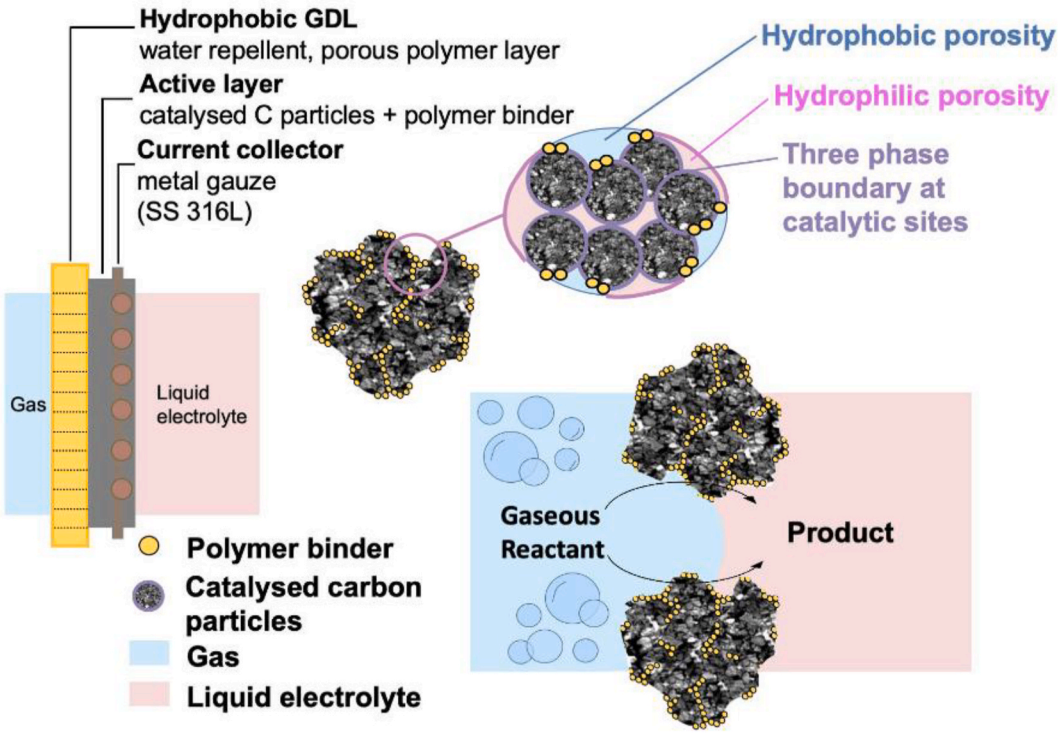

Fig. 8. GDE electrode structure encompassing the hydrophobic GDL, active layer and current collector. Reprinted with permission from Horizon SPIRE Project PERFORM website https://performproject.eu/archivos/2290.

absolve. The hydrophilic (slightly hydrophobic) zone must be wetted by the electrolyte to allow the protons within the electrolyte to travel to the catalytic sites. If the first region/zone were of a super hydrophobic-type, proton mass transfer resistance would have occurred affecting negatively the cathode performance. On the contrary, the second region/-zone must be of super hydrophobic type to be electrolyte-free and guarantee the presence of oxygen from the atmosphere [229]. If the super hydrophobicity of the second region would have been compromised or was not enough efficient, electrolyte would fill the pores of the entire electrode not allowing oxygen circulation within the electrode. This undesired situation is called "cathode flooding" and limits severely the cathode performance due to the availability of oxygen only as dissolved O_2 [230]. This cathode architecture creates a hydrophilic/hydrophobic gradient that enhances natural air circulation within the structure.

The air-breathing cathode architecture is specifically engineered to enhance the three-phase interface (TPI) crucial for efficient ORR. This design optimizes the interaction of the liquid phase (responsible for proton transport), the gaseous phase (ensuring oxygen availability and enhancing oxygen transport), and the solid phase (facilitating electron transport through the cathode support). Typically, these cathodes feature a pellet-type structure composed of carbonaceous conductive materials such as teflonized carbon black or activated carbon, layered over a carbonaceous or metallic porous current collector. This integrated design aims to maximize performance for both enzymes and inorganic electrocatalysts by optimizing the operational conditions within the cathode structure [231].

At the same time, a diffusion layer or multiple layers may be introduced on the air-facing side of the current collector. Examples of diffusion layers made of PTFE (polytetrafluoroethylene), PDMS (Polydimethylsiloxane), or other polymers are frequently reported. Importantly, this layer does not allow water/electrolyte permeation through the cathode structure. In fact, in case of mechanical structure failure, or the creation of liquid preferential pathways through the pellet-type cathode, MFC ceases to function due to leakage of the anode electrolyte. The addition of diffusion layers is crucial to keep the integrity of the system that is supposed to work continuously for long-term operations. Moreover, being permeable to oxygen, this hydrophobic layer might increase the hydrophobic gradient within the cathode structure and therefore might be beneficial for the ORR [232].

For a very long time, the research on BESs was restricted to lab-scale systems with electrode sizes ranging from a few cm^2 to some hundred cm^2 [233]. If the objective was developing and screening novel electrocatalysts for ORR, the small-scale systems served well as ideal tools allowing for rapid testing and saving time and costs. However, as the efficiencies improved, the need for demonstration at a large scale also became obvious. One tangible approach of upscaling from the power production point of view is stacking several small to medium-sized individual MFCs in series or parallel [234,235]. However, from a combined wastewater treatment perspective, this is not the most practical approach requiring larger single modules that correspond to larger electrodes (to serve as anode and cathode) as well as membranes/separators. The conventional cathode designs for MFCs such as microfiltration or ultrafiltration flat sheet cathodes suffer from limited cathode packing density. There are two main challenges with the geometric enlargement of GDEs. While on one hand, with increasing dimensions, it is difficult to keep the air compartment dry due to the possibility of the leakage of electrolyte from the gas diffusion layer (mechanical weakness of the electrode), at the same time, the current distribution across the whole surface of the electrode may become skewed and the sections of the electrode in the middle becoming disadvantaged compared to the edges (ohmic losses during operation) [236]. To overcome this, recently, large-scale GDEs were developed at VITO and independently tested in two different laboratories. These novel multi-panel cathodes contained several smaller cathodes welded into a single metal sheet, much like windows are made of many panes of glass [186]. This was tested in an 85 L reactor and was compared to a small cell with an 11.3 cm^2 electrode and a medium cell with a 52 cm^2 electrode. Afterwards, the biggest ever-investigated scale multi-panel SS/AC cathodes were tested in a submergible 255 L prototype MFC module using municipal wastewater [237]. This type of electrodes, available under the trade names VITO CORE® and VITO CASE®, are quite flexible and can be shaped as a tubular GDE as well as a single unit or in use inside an artistic version of a living lamp, named as "Spark of life" based on the MFC principle [238]. Up to now, to the best of our knowledge, there is a single company in the world that is commercializing large scale MFCs named AQUACYCL LLD, USA.

7. Conclusions and outlooks

ORR is crucial in electrochemistry, playing a key role in energy conversion and storage in a variety of (bio)electrochemical reactions. BESs offer benefits like energy harvesting from waste, wastewater treatment, low-energy desalination, environmental remediation, and biosensing [239,240]. Designing ORR electrocatalysts and electrodes for BESs is as important as the biotic components, deserving special attention due to its potential as a rate-limiting process [47]. Effective ORR in neutral media is essential, presenting both challenges and opportunities at realistic technology scales.

Key issues for large-scale BESs include cost, durability, power density, biosensing, and organic/pollutants degradation [23,241]. In BESs and electrochemical energy storage systems, the ORR, in the majority of cases, limits the output performance. Improving ORR activity and durability requires balancing these issues. Inorganic, enzymatic, and microbial electrocatalysts each have their pros and cons. Substantial progress has been achieved in the field of PGM-free electrocatalysts, which now show improved activity and stability compared to a decade ago.

Inorganic electrocatalysts, especially PGM cathodes, are well-established for acidic and alkaline media but are costly and less durable in BESs. The development of PGM-free electrocatalysts for FCs has renewed interest in understanding ET mechanisms, aiming for activity and durability improvements. Carbonaceous materials, offering a balance of cost, activity, and durability, are commonly used in BESs. TM–N–C electrocatalysts, belonging to the family of PGM-free electrocatalysts, show promise but need further development to enhance their active sites and accessibility [242].

Enzymatic electrocatalysts, particularly MCOs, have been deeply studied for their ET mechanisms, leading to a new generation of EFCs with high selectivity and minimal side reactions. However, they have a short operational lifetime, necessitating advancements in interfacial ET and storage stability. Research in this area focuses on bioengineering electrodes and improving immobilization techniques [243,244].

Electroactive biofilms that catalyze ORR still require the study of model aerobic bacteria, although they are rare and their electroactivity is unpredictable. Research into bacterial ET mechanisms, synthetic co-cultures and reconstructed biofilms can provide insights into their fundamental mechanisms of action and interactions both cellular and with electrode surfaces. Innovations are needed to overcome the limitation of low oxygen solubility in water and improve the microbial density of biofilms on electrodes [172]. Major technological leaps could be made by directing research efforts towards the use of synthetic dry microbial biofilms and the direct conversion of atmospheric oxygen.

Cathode architecture is crucial for BES performance, with ORR electrocatalyst activity not always translating into high performance once integrated into an electrode. Optimized cathode designs, incorporating hydrophilic and hydrophobic features, guaranteeing a TPI, are essential for practical BES applications. Scaling up and manufacturing air-breathing gas diffusion electrodes require cost-effective techniques, possibly involving multiple medium-sized cathodes or roll-to-roll fabrication [245].

Moreover, exploring the effect of a magnetic field on ORR will unveil

new prospects for developing more efficient electrocatalysts, substantially boosting at least by 50 % the diffusion-limited reaction mainly due to ions whirling motion under Lorentz forces [246].

As biocathodes evolve and integrate into devices, addressing engineering and design issues will enhance ORR kinetics in neutral media, contributing to the success of BES technology.

CRediT authorship contribution statement

Angelo Tricase: Writing – original draft, Conceptualization. **Mohsin Muhyuddin:** Writing – review & editing, Conceptualization. **Benjamin Erable:** Writing – review & editing, Conceptualization. **Plamen Atanassov:** Writing – review & editing, Conceptualization. **Deepak Pant:** Writing – review & editing, Conceptualization. **Carlo Santoro:** Writing – review & editing, Writing – original draft, Funding acquisition, Conceptualization. **Paolo Bollella:** Writing – review & editing, Writing – original draft, Funding acquisition, Conceptualization.

Declaration of competing interest

The authors declare that they have no known competing financial interests or personal relationships that could have appeared to influence the work reported in this paper.

Acknowledgments

P. B. and A. T. acknowledge the European Union under the Italian National Recovery and Resilience Plan (NRRP) of NextGenerationEU, partnership on “Telecommunications of the Future” (PE00000001 - program “RESTART”, Structural Project DREAMS), and CSGI (Centre for Colloid and Surface Science). C.S. would like to acknowledge the funding by the European Union – NextGeneration EU from the Italian Ministry of Environment and Energy Security POR H2 AdP MMES/ENEA with involvement of CNR and RSE, PNRR - Mission 2, Component 2, Investment 3.5 "Ricerca e sviluppo sull’idrogeno” ENEA – UNIMIB agreement (Procedure 1.1.3 PNRR POR H2).

Data availability

No data was used for the research described in the article.

References

[1] P. Trogadas, M.-O. Coppens, Nature-inspired electrocatalysts and devices for energy conversion, Chem. Soc. Rev. 49 (2020) 3107–3141.
[2] M. Li, X. Bi, R. Wang, Y. Li, G. Jiang, L. Li, C. Zhong, Z. Chen, J. Lu, Relating catalysis between fuel cell and metal-air batteries, Matter 2 (2020) 32–49.
[3] L. Lin, N. Miao, G.G. Wallace, J. Chen, D.A. Allwood, Engineering carbon materials for electrochemical oxygen reduction reactions, Adv. Energy Mater. 11 (2021) 2100695.
[4] S. Huang, Q. Wang, Redox-mediated oxygen electrochemistry and the materials aspects, Acc. Mater. Res. 4 (2023) 693–703.
[5] H. Chen, O. Simoska, K. Lim, M. Grattieri, M. Yuan, F. Dong, Y.S. Lee, K. Beaver, S. Weliwatte, E.M. Gaffney, Fundamentals, applications, and future directions of bioelectrocatalysis, Chem. Rev. 120 (2020) 12903–12993.
[6] J. Li, Z. Chen, Revitalizing microbial fuel cells: a comprehensive review on the transformative role of iron-based materials in electrode design and catalyst development, Chem. Eng. J. (2024) 151323.
[7] R.N.P. Colombo, G.C. Sedenho, F.N. Crespilho, Challenges in biomaterials science for electrochemical biosensing and bioenergy, Chem. Mater. 34 (2022) 10211–10222.
[8] M.A. Costa de Oliveira, A. D'Epifanio, H. Ohnuki, B. Mecheri, Platinum group metal-free catalysts for oxygen reduction reaction: applications in microbial fuel cells, Catalysts 10 (2020) 475.
[9] T. Vo, J. Gao, Y. Liu, Recent development and future frontiers of oxygen reduction reaction in neutral media and seawater, Adv. Funct. Mater. 34 (2024) 2314282.
[10] Y.-Y. Zhao, W. Yu, X. Sun, H. Huang, F. Li, M. Luo, Harnessing electrolyte chemistry to advance oxygen reduction catalysis for fuel cells and electrosynthesis, ACS Catal. 14 (2024) 16963–16985.
[11] S. Li, L. Shi, Y. Guo, J. Wang, D. Liu, S. Zhao, Selective oxygen reduction reaction: mechanism understanding, catalyst design and practical application, Chem. Sci. 15 (2024) 11188–11228.
[12] J. Zhang, H.B. Yang, D. Zhou, B. Liu, Adsorption energy in oxygen electrocatalysis, Chem. Rev. 122 (2022) 17028–17072.
[13] Z. Kou, X. Li, L. Zhang, W. Zang, X. Gao, J. Wang, Dynamic surface chemistry of catalysts in oxygen evolution reaction, Small Science 1 (2021) 2100011.
[14] N. Ramaswamy, S. Mukerjee, Influence of Inner- and outer-sphere electron transfer mechanisms during electrocatalysis of oxygen reduction in alkaline media, J. Phys. Chem. C 115 (2011) 18015–18026.
[15] X. Ge, A. Sumboja, D. Wuu, T. An, B. Li, F.W.T. Goh, T.S.A. Hor, Y. Zong, Z. Liu, Oxygen reduction in alkaline media: from mechanisms to recent advances of catalysts, ACS Catal. 5 (2015) 4643–4667.
[16] V. Briega-Martos, E. Herrero, J.M. Feliu, Effect of pH and water structure on the oxygen reduction reaction on platinum electrodes, Electrochim. Acta 241 (2017) 497–509.
[17] M.R. Tarasevich, O.V. Korchagin, Electrocatalysis and pH (a review), Russ. J. Electrochem. 49 (2013) 600–618.
[18] D.-W. Wang, D. Su, Heterogeneous nanocarbon materials for oxygen reduction reaction, Energy Environ. Sci. 7 (2014) 576–591.
[19] V. Briega-Martos, W. Cheuquepán, J.M. Feliu, Detection of superoxide anion oxygen reduction reaction intermediate on Pt(111) by infrared reflection absorption spectroscopy in neutral pH conditions, J. Phys. Chem. Lett. 12 (2021) 1588–1592.
[20] S.C. Popat, D. Ki, M.N. Young, B.E. Rittmann, C.I. Torres, Buffer p K_a and transport govern the concentration overpotential in electrochemical oxygen reduction at neutral pH, Chemelectrochem 1 (2014) 1909–1915.
[21] Y. Pang, H. Xie, Y. Sun, M.-M. Titirici, G.-L. Chai, Electrochemical oxygen reduction for H 2 O 2 production: catalysts, pH effects and mechanisms, J. Mater. Chem. A 8 (2020) 24996–25016.
[22] Y. Tian, D. Deng, L. Xu, M. Li, H. Chen, Z. Wu, S. Zhang, Strategies for sustainable production of hydrogen peroxide via oxygen reduction reaction: from catalyst design to device setup, Nano-Micro Lett. 15 (2023) 122.
[23] S. Bajracharya, M. Sharma, G. Mohanakrishna, X.D. Benneton, D.P. Strik, P. M. Sarma, D. Pant, An overview on emerging bioelectrochemical systems (BESs): technology for sustainable electricity, waste remediation, resource recovery, chemical production and beyond, Renew. Energy 98 (2016) 153–170.
[24] S. Wang, E. Zhu, Y. Huang, H. Heinz, Direct correlation of oxygen adsorption on platinum-electrolyte interfaces with the activity in the oxygen reduction reaction, Sci. Adv. 7 (2021) eabb1435.
[25] S.D. Bhoyate, J. Kim, F.M. de Souza, J. Lin, E. Lee, A. Kumar, R.K. Gupta, Science and engineering for non-noble-metal-based electrocatalysts to boost their ORR performance: a critical review, Coord. Chem. Rev. 474 (2023) 214854.
[26] Y. Pang, K. Wang, H. Xie, Y. Sun, M.-M. Titirici, G.-L. Chai, Mesoporous carbon hollow spheres as efficient electrocatalysts for oxygen reduction to hydrogen peroxide in neutral electrolytes, ACS Catal. 10 (2020) 7434–7442.
[27] I. Bento, L.O. Martins, G.G. Lopes, M.A. Carrondo, P.F. Lindley, Dioxygen reduction by multi-copper oxidases; a structural perspective, Dalton Trans. (2005) 3507–3513.
[28] E.I. Solomon, A.J. Augustine, J. Yoon, O 2 reduction to H2O by the multicopper oxidases, Dalton Trans. (2008) 3921–3932.
[29] S. Dey, B. Mondal, S. Chatterjee, A. Rana, S. Amanullah, A. Dey, Molecular electrocatalysts for the oxygen reduction reaction, Nat. Rev. Chem 1 (2017) 1–20.
[30] Z. He, Y. Huang, A.K. Manohar, F. Mansfeld, Effect of electrolyte pH on the rate of the anodic and cathodic reactions in an air-cathode microbial fuel cell, Bioelectrochemistry 74 (2008) 78–82.
[31] F. Zhao, F. Harnisch, U. Schröder, F. Scholz, P. Bogdanoff, I. Herrmann, Challenges and constraints of using oxygen cathodes in microbial fuel cells, Environmental Science & Technology 40 (2006) 5193–5199.
[32] D.R. Bond, D.R. Lovley, Electricity production by *Geobacter sulfurreducens* attached to electrodes, Appl. Environ. Microbiol. 69 (2003) 1548–1555.
[33] Y. Zhao, D.P. Adiyeri Saseendran, C. Huang, C.A. Triana, W.R. Marks, H. Chen, H. Zhao, G.R. Patzke, Oxygen evolution/reduction reaction catalysts: from in situ monitoring and reaction mechanisms to rational design, Chem. Rev. 123 (2023) 6257–6358.
[34] S.C. Perry, G. Denuault, The oxygen reduction reaction (ORR) on reduced metals: evidence for a unique relationship between the coverage of adsorbed oxygen species and adsorption energy, Phys. Chem. Chem. Phys. 18 (2016) 10218–10223.
[35] N.M. Marković, H.A. Gasteiger, B.N. Grgur, P.N. Ross, Oxygen reduction reaction on Pt(111): effects of bromide, J. Electroanal. Chem. 467 (1999) 157–163.
[36] X. Wang, H. Zhong, S. Xi, W.S.V. Lee, J. Xue, Understanding of oxygen redox in the oxygen evolution reaction, Adv. Mater. 34 (2022) 2107956.
[37] M. Shao, P. Liu, R.R. Adzic, Superoxide anion is the intermediate in the oxygen reduction reaction on platinum electrodes, J. Am. Chem. Soc. 128 (2006) 7408–7409.
[38] A. Kulkarni, S. Siahrostami, A. Patel, J.K. Nørskov, Understanding catalytic activity trends in the oxygen reduction reaction, Chem. Rev. 118 (2018) 2302–2312.
[39] N. Mano, A. de Poulpiquet, O2 reduction in enzymatic biofuel cells, Chem. Rev. 118 (2017) 2392–2468.
[40] H. Yuan, Y. Hou, I.M. Abu-Reesh, J. Chen, Z. He, Oxygen reduction reaction catalysts used in microbial fuel cells for energy-efficient wastewater treatment: a review, Mater. Horiz. 3 (2016) 382–401.
[41] W. Zhou, H. Su, W. Cheng, Y. Li, J. Jiang, M. Liu, F. Yu, W. Wang, S. Wei, Q. Liu, Regulating the scaling relationship for high catalytic kinetics and selectivity of the oxygen reduction reaction, Nat. Commun. 13 (2022) 6414.

[42] Y. Wang, G.I.N. Waterhouse, L. Shang, T. Zhang, Electrocatalytic oxygen reduction to hydrogen peroxide: from homogeneous to heterogeneous electrocatalysis, Adv. Energy Mater. 11 (2021) 2003323.

[43] Z. Peng, Y. Chen, P.G. Bruce, Y. Xu, Direct detection of the superoxide anion as a stable intermediate in the electroreduction of oxygen in a non-aqueous electrolyte containing phenol as a proton source, Angew. Chem. 127 (2015) 8283–8286.

[44] S. Mondal, D. Bagchi, M. Riyaz, S. Sarkar, A.K. Singh, C.P. Vinod, S.C. Peter, In situ mechanistic insights for the oxygen reduction reaction in chemically modulated ordered intermetallic catalyst promoting complete electron transfer, J. Am. Chem. Soc. 144 (2022) 11859–11869.

[45] K. Yuan, H. Li, X. Gu, Y. Zheng, X. Wu, Y. Zhao, J. Zhou, S. Cui, Electrocatalysts for the formation of hydrogen peroxide by oxygen reduction reaction, ChemSusChem (2024) e202401952.

[46] E.C. Tse, C.J. Barile, N.A. Kirchschlager, Y. Li, J.P. Gewargis, S.C. Zimmerman, A. Hosseini, A.A. Gewirth, Proton transfer dynamics control the mechanism of O2 reduction by a non-precious metal electrocatalyst, Nat. Mater. 15 (2016) 754–759.

[47] C. Santoro, P. Bollella, B. Erable, P. Atanassov, D. Pant, Oxygen reduction reaction electrocatalysis in neutral media for bioelectrochemical systems, Nat. Catal. 5 (2022) 473–484.

[48] S.K. Singh, K. Takeyasu, J. Nakamura, Active sites and mechanism of oxygen reduction reaction electrocatalysis on nitrogen-doped carbon materials, Adv. Mater. 31 (2019) 1804297.

[49] V. Tripković, E. Skúlason, S. Siahrostami, J.K. Nørskov, J. Rossmeisl, The oxygen reduction reaction mechanism on Pt (1 1 1) from density functional theory calculations, Electrochim. Acta 55 (2010) 7975–7981.

[50] P.R. Norton, K. Griffiths, P.E. Bindner, Interaction of O2 with Pt (100): II. Kinetics and energetics, Surf. Sci. 138 (1984) 125–147.

[51] On the magnetic properties of some haemoglobin complexes, Proc. R. Soc. Lond. A 235 (1956) 23–36.

[52] L. Pauling, Nature of the iron–oxygen bond in oxyhaemoglobin, Nature 203 (1964) 182–183.

[53] E. Yeager, Recent advances in the science of electrocatalysis, J. Electrochem. Soc. 128 (1981) 160C.

[54] E. Yeager, Electrocatalysts for O2 reduction, Electrochim. Acta 29 (1984) 1527–1537.

[55] X. Li, D. Wang, S. Zha, Y. Chu, L. Pan, M. Wu, C. Liu, W. Wang, N. Mitsuzaki, Z. Chen, Active sites identification and engineering of M-N-C electrocatalysts toward oxygen reduction reaction, Int. J. Hydrogen Energy 51 (2024) 1110–1127.

[56] E.I. Solomon, U.M. Sundaram, T.E. Machonkin, Multicopper oxidases and oxygenases, Chem. Rev. 96 (1996) 2563–2606.

[57] S. Freguia, S. Tsujimura, K. Kano, Electron transfer pathways in microbial oxygen biocathodes, Electrochim. Acta 55 (2010) 813–818.

[58] S. Rojas-Carbonell, K. Artyushkova, A. Serov, C. Santoro, I. Matanovic, P. Atanassov, Effect of pH on the activity of platinum group metal-free catalysts in oxygen reduction reaction, ACS Catal. 8 (2018) 3041–3053.

[59] G. Bae, M.W. Chung, S.G. Ji, F. Jaouen, C.H. Choi, pH effect on the H_2 O_2 -Induced deactivation of Fe-N-C catalysts, ACS Catal. 10 (2020) 8485–8495.

[60] V. Gueskine, M. Vagin, M. Berggren, X. Crispin, I. Zozoulenko, Oxygen reduction reaction at conducting polymer electrodes in a wider context: insights from modelling concerning outer and inner sphere mechanisms, Electrochemical Science Adv 3 (2023) e2100191.

[61] S. Strbac, The effect of pH on oxygen and hydrogen peroxide reduction on polycrystalline Pt electrode, Electrochim. Acta 56 (2011) 1597–1604.

[62] S.T. Putnam, J. Rodríguez-López, Real-time investigation of reactive oxygen species and radicals evolved from operating Fe–N–C electrocatalysts during the ORR: potential dependence, impact on degradation, and structural comparisons, Chem. Sci. 15 (2024) 10036–10045.

[63] F. Armillotta, D. Bidoggia, S. Baronio, P. Biasin, A. Annese, M. Scardamaglia, S. Zhu, B. Bozzini, S. Modesti, M. Peressi, E. Vesselli, Single metal atom catalysts and ORR: H-bonding, solvation, and the elusive hydroperoxyl intermediate, ACS Catal. 12 (2022) 7950–7959.

[64] F. Armillotta, D. Bidoggia, S. Baronio, A. Sala, R. Costantini, M. dell'Angela, I. Cojocariu, V. Feyer, A. Morgante, M. Peressi, E. Vesselli, Co(III), Co(II), Co(I): tuning single cobalt metal atom oxidation states in a 2D coordination network, Adv. Funct. Mater. 34 (2024) 2408200.

[65] J. Timoshenko, B. Roldan Cuenya, *In situ/operando* electrocatalyst characterization by X-ray absorption spectroscopy, Chem. Rev. 121 (2021) 882–961.

[66] Y. Yang, Y. Xiong, R. Zeng, X. Lu, M. Krumov, X. Huang, W. Xu, H. Wang, F. J. DiSalvo, JoelD. Brock, D.A. Muller, H.D. Abruña, Operando methods in electrocatalysis, ACS Catal. 11 (2021) 1136–1178.

[67] J. Li, J. Gong, Operando characterization techniques for electrocatalysis, Energy Environ. Sci. 13 (2020) 3748–3779.

[68] J.-C. Dong, X.-G. Zhang, V. Briega-Martos, X. Jin, J. Yang, S. Chen, Z.-L. Yang, D.-Y. Wu, J.M. Feliu, C.T. Williams, In situ raman spectroscopic evidence for oxygen reduction reaction intermediates at platinum single-crystal surfaces, Nat. Energy 4 (2019) 60–67.

[69] J.K. Nørskov, J. Rossmeisl, A. Logadottir, L. Lindqvist, J.R. Kitchin, T. Bligaard, H. Jónsson, Origin of the overpotential for oxygen reduction at a fuel-cell cathode, J. Phys. Chem. B 108 (2004) 17886–17892.

[70] V. Stamenkovic, B.S. Mun, K.J.J. Mayrhofer, P.N. Ross, N.M. Markovic, J. Rossmeisl, J. Greeley, J.K. Nørskov, Changing the activity of electrocatalysts for oxygen reduction by tuning the surface electronic structure, Angew. Chem. Int. Ed. 45 (2006) 2897–2901.

[71] H.A. Hansen, V. Viswanathan, J.K. Nørskov, Unifying kinetic and thermodynamic analysis of 2 e^- and 4 e^- reduction of oxygen on metal surfaces, J. Phys. Chem. C 118 (2014) 6706–6718.

[72] J. Chen, L. Fang, S. Luo, Y. Liu, S. Chen, Electrocatalytic O_2 reduction on pt: multiple roles of oxygenated adsorbates, nature of active sites, and origin of overpotential, J. Phys. Chem. C 121 (2017) 6209–6217.

[73] R. Kothalam, R. Kalidass, Activity descriptors for atomically precise oxygen reduction reaction (ORR) electrocatalysts, in: A. Kumar, R.K. Gupta (Eds.), Atomically Precise Electrocatalysts for Electrochemical Energy Applications, Springer Nature Switzerland, Cham, 2024, pp. 147–168.

[74] A. Kulkarni, S. Siahrostami, A. Patel, J.K. Nørskov, Understanding catalytic activity trends in the oxygen reduction reaction, Chem. Rev. 118 (2018) 2302–2312.

[75] A.E. Thorarinsdottir, D.P. Erdosy, C. Costentin, J.A. Mason, D.G. Nocera, Enhanced activity for the oxygen reduction reaction in microporous water, Nat. Catal. 6 (2023) 425–434.

[76] J. Lv, Z. Lang, J. Fu, Q. Lan, R. Liu, H. Zang, Y. Li, D. Ye, C. Streb, Molecular iron oxide clusters boost the oxygen reduction reaction of platinum electrocatalysts at near-neutral pH, Angew. Chem. 134 (2022) e202202650.

[77] X. Wu, L. Liu, K. Yuan, Y. Shao, X. Shen, S. Cui, X. Chen, Modulating electronic structure and atomic insights into the novel hierarchically porous PdCuFe trimetallic alloy aerogel for efficient oxygen reduction, Small 20 (2024) 2307243.

[78] V.C.A. Ficca, C. Santoro, E. Placidi, F. Arciprete, A. Serov, P. Atanassov, B. Mecheri, Exchange current density as an effective descriptor of poisoning of active sites in platinum group metal-free electrocatalysts for oxygen reduction reaction, ACS Catal. 13 (2023) 2162–2175.

[79] V.C.A. Ficca, C. Santoro, A. D'Epifanio, S. Licoccia, A. Serov, P. Atanassov, B. Mecheri, Effect of active site poisoning on iron−Nitrogen−Carbon platinum-group-metal-free oxygen reduction reaction catalysts operating in neutral media: a rotating disk electrode study, Chemelectrochem 7 (2020) 3044–3055.

[80] V.C.A. Ficca, C. Santoro, E. Marsili, W. da Silva Freitas, A. Serov, P. Atanassov, B. Mecheri, Sensing nitrite by iron-nitrogen-carbon oxygen reduction electrocatalyst, Electrochim. Acta 402 (2022) 139514.

[81] S.A. Mirshokraee, M. Muhyuddin, R. Lorenzi, G. Tseberlidis, C.L. Vecchio, V. Baglio, E. Berretti, A. Lavacchi, C. Santoro, Litchi-derived platinum group metal-free electrocatalysts for oxygen reduction reaction and hydrogen evolution reaction in alkaline media, SusMat 3 (2023) 248–262.

[82] B. Mecheri, R. Gokhale, C. Santoro, M.A. Costa De Oliveira, A. D'Epifanio, S. Licoccia, A. Serov, K. Artyushkova, P. Atanassov, Oxygen reduction reaction electrocatalysts derived from iron salt and benzimidazole and aminobenzimidazole precursors and their application in microbial fuel cell cathodes, ACS Appl. Energy Mater. 1 (2018) 5755–5765.

[83] M. Kodali, R. Gokhale, C. Santoro, A. Serov, K. Artyushkova, P. Atanassov, High performance platinum group metal-free cathode catalysts for microbial fuel cell (MFC), J. Electrochem. Soc. 164 (2016) H3041.

[84] C. Santoro, M. Kodali, N. Shamoon, A. Serov, F. Soavi, I. Merino-Jimenez, I. Gajda, J. Greenman, I. Ieropoulos, P. Atanassov, Increased power generation in supercapacitive microbial fuel cell stack using FeNC cathode catalyst, J. Power Sources 412 (2019) 416–424.

[85] C. Santoro, A. Serov, K. Artyushkova, P. Atanassov, Platinum group metal-free oxygen reduction electrocatalysts used in neutral electrolytes for bioelectrochemical reactor applications, Curr. Opin. Electrochem. 23 (2020) 106–113.

[86] C. Liang, X. Han, T. Zhang, B. Dong, Y. Li, Z. Zhuang, A. Han, J. Liu, Cu nanoclusters accelerate the rate-determining step of oxygen reduction on fe—n—c in all pH range, Adv. Energy Mater. 14 (2024) 2303935.

[87] C. Shao, L. Wu, H. Zhang, Q. Jiang, X. Xu, Y. Wang, S. Zhuang, H. Chu, L. Sun, J. Ye, B. Li, X. Wang, A versatile approach to boost oxygen reduction of $Fe\text{-}N_4$ sites by controllably incorporating sulfur functionality, Adv. Funct. Mater. 31 (2021) 2100833.

[88] Y. Li, H. Cheng, M. Wang, J. Xu, L. Guan, Highly coordinative molecular cobalt–phthalocyanine electrocatalyst on an oxidized single-walled carbon nanotube for efficient hydrogen peroxide production, Mater. Horiz. 11 (2024) 2517–2527.

[89] L. Wang, Q. An, X. Sheng, Z. Mei, Q. Jing, X. Zhao, Q. Xu, L. Duan, X. Zou, H. Guo, Modulation of electronic spin state and construction of dual-atomic tandem reaction for enhanced pH-universal oxygen reduction, Appl. Catal. B Environ. 343 (2024) 123509.

[90] Y. Wang, L. Wu, K. Qu, B. Li, Atomically dispersed FeN4 and Fe2P nanoparticles anchored in N, P-codoped hollow porous carbon for efficient oxygen reduction reaction, Fuel 380 (2025) 133072.

[91] S. Ji, Y. Wang, H. Liu, X. Lu, C. Guo, S. Xin, J.H. Horton, F. Zhan, Y. Wang, Z. Li, Regulating the electronic synergy of asymmetric atomic Fe sites with adjacent defects for boosting activity and durability toward oxygen reduction, Adv. Funct. Mater. 34 (2024) 2314621.

[92] N.E.G. Ligthart, P.H. Van Langevelde, J.T. Padding, D.G.H. Hetterscheid, D. A. Vermaas, 20-Fold increased limiting currents in oxygen reduction with Cu-tmpa by replacing Flow-By with flow-through electrodes, ACS Sustainable Chem. Eng. 12 (2024) 12909–12918.

[93] J. Cheng, X. Tu, L. Zhang, M. Han, R. Zhou, S. Luo, H. Zeng, T. Li, J. Zou, A novel bifunctional particle electrode with abundant Fe/Fe3C and Fe-NC sites to enhance the performance of electro-Fenton in degrading organic pollutant, J. Environ. Chem. Eng. 12 (2024) 112902.

[94] S. Sato-Soto, S. Sato, S. Tsujimura, Performance of a Fe-NC catalyst in single-chamber MFC air-cathode at neutral media, Electrochemistry 92 (2024), 022016–022016.

[95] Y. Zhang, Y. Dong, Y. Wu, X. Zhong, Y. Song, K. Wang, Q. Shi, T. Ma, H. Liu, J. Liang, H. Fei, Atomically dispersed Cu nanostructures with pH-Universal electrocatalytic oxygen reduction activity for Zn–Air batteries, ACS Appl. Nano Mater. 6 (2023) 18548–18557.

[96] W. Xue, Q. Zhou, X. Cui, J. Zhang, S. Zuo, F. Mo, J. Jiang, X. Zhu, Z. Lin, Atomically dispersed FeN_2 P_2 motif with high activity and stability for oxygen reduction reaction over the entire pH range, Angew. Chem. Int. Ed. 62 (2023) e202307504.

[97] E.O. Nyangau, H. Abe, Y. Nakayasu, M. Umetsu, M. Watanabe, C. Tada, Iron azaphthalocyanine electrocatalysts for enhancing oxygen reduction reactions under neutral conditions and power density in microbial fuel cells, Bioresour. Technol. Rep. 23 (2023) 101565.

[98] B. Li, Q. Li, X. Wang, Iron/iron carbide coupled with S, N co-doped porous carbon as effective oxygen reduction reaction catalyst for microbial fuel cells, Environ. Res. 228 (2023) 115808.

[99] L. Li, N. Li, J.-W. Xia, S.-L. Zhou, X.-Y. Qian, F.-X. Yin, G.-H. Dai, G.-Y. He, H.-Q. Chen, A pH-universal ORR catalyst with atomic Fe-heteroatom (N, S) sites for high-performance Zn-air batteries, Nano Res. 16 (2023) 9416–9425.

[100] S. Tang, Q. Liu, L. Zhang, Bio-assisted atomically dispersed fe–n–c electrocatalyst with ultra-low Fe loading toward pH-Universal oxygen reduction reaction and neutral Zn-Air battery, ACS Sustainable Chem. Eng. 11 (2023) 8131–8139.

[101] H. Zhang, Y. Wang, T. Wu, J. Yu, S.R.B. Arulmani, W. Chen, L. Huang, M. Su, J. Yan, X. Liu, Rational design of porous Fex-N@ MOF as a highly efficient catalyst for oxygen reduction over a wide pH range, J. Alloys Compd. 944 (2023) 169039.

[102] M. Gong, A. Mehmood, B. Ali, K.-W. Nam, A. Kucernak, Oxygen reduction reaction activity in non-precious single-atom (M–N/C) catalysts—contribution of metal and carbon/nitrogen framework-based sites, ACS Catal. 13 (2023) 6661–6674.

[103] C. Ye, Y. Zhou, H. Li, Y. Shen, Single-iron, cobalt, nickel, and copper-atom catalysts for the selective reduction of oxygen to H 2 O 2, Green Chem. 25 (2023) 3931–3939.

[104] Z. Li, S. Ji, C. Xu, L. Leng, H. Liu, J.H. Horton, L. Du, J. Gao, C. He, X. Qi, Q. Xu, J. Zhu, Engineering the electronic structure of single-atom iron sites with boosted oxygen bifunctional activity for zinc–air batteries, Adv. Mater. 35 (2023) 2209644.

[105] Y. Irmawati, F. Balqis, F. Destyorini, C.G. Adios, R. Yudianti, F. Iskandar, A. Sumboja, Cobalt nanoparticles encapsulated with N-Doped bamboo-like carbon nanofibers as bifunctional catalysts for oxygen reduction/evolution reactions in a wide pH range, ACS Appl. Nano Mater. 6 (2023) 2708–2718.

[106] F. Ding, H. Liu, X. Jiang, Y. Jiang, J. Cheng, Y. Tu, W. Xiao, C. Li, X. Yan, Bimetallic zeolite imidazolium framework derived multiphase Co/HNC as pH-universal catalysts with efficient oxygen reduction performance for microbial fuel cells, Electrochim. Acta 438 (2023) 141548.

[107] H.M. Sabaa, K.M. El-Khatib, M.Y. El-Kady, S.A. Mahmoud, Spinel structure of activated carbon supported MFe2O4 composites as an economic and efficient electrocatalyst for oxygen reduction reaction in neutral media, J. Solid State Electrochem. 26 (2022) 2749–2763.

[108] C. Fang, Q. Yi, A. Chen, Y. Wang, Y. Wang, X. Li, Fabrication of FeCo/multidimensional carbon-based nanocomposites as excellent cathodic catalysts of Zn-air battery, J. Electrochem. Soc. 169 (2022) 110538.

[109] Y. Dong, Z. Fang, D. Ou, Q. Shi, Y. Ma, W. Yang, B. Tang, Q. Liu, Rational fabrication of S-modified fe–n–c nanosheet electrocatalysts for efficient and stable pH-universal oxygen reduction, Chem. Eng. J. 444 (2022) 136433.

[110] T. He, Y. Chen, Q. Liu, B. Lu, X. Song, H. Liu, M. Liu, Y. Liu, Y. Zhang, X. Ouyang, S. Chen, Theory-guided regulation of FeN_4 spin state by neighboring Cu atoms for enhanced oxygen reduction electrocatalysis in flexible metal–air batteries, Angew. Chem. 134 (2022) e202201007.

[111] Y. Liu, S. He, B. Huang, Z. Kong, L. Guan, Influence of different Fe doping strategies on modulating active sites and oxygen reduction reaction performance of Fe, N-doped carbonaceous catalysts, J. Energy Chem. 70 (2022) 511–520.

[112] Y. Gong, Y. Xu, Y. Que, X. Xu, Y. Tang, D. Ye, H. Zhao, J. Zhang, Prussian blue analogues derived electrocatalyst with multicatalytic centers for boosting oxygen reduction reaction in the wide pH range, J. Colloid Interface Sci. 612 (2022) 639–649.

[113] M. Zhao, H. Liu, H. Zhang, W. Chen, H. Sun, Z. Wang, B. Zhang, L. Song, Y. Yang, C. Ma, Y. Han, W. Huang, A pH-universal ORR catalyst with single-atom iron sites derived from a double-layer MOF for superior flexible quasi-solid-state rechargeable Zn–air batteries, Energy Environ. Sci. 14 (2021) 6455–6463.

[114] A. Iannaci, S. Ingle, C. Domínguez, M. Longhi, O. Merdrignac-Conanec, S. Ababou-Girard, F. Barrière, P.E. Colavita, Nanoscaffold effects on the performance of air-cathodes for microbial fuel cells: sustainable Fe/N-carbon electrocatalysts for the oxygen reduction reaction under neutral pH conditions, Bioelectrochemistry 142 (2021) 107937.

[115] L. Yan, L. Xie, X.-L. Wu, M. Qian, J. Chen, Y. Zhong, Y. Hu, Precise regulation of pyrrole-type single-atom Mn-N4 sites for superior pH-universal oxygen reduction, Carbon Energy 3 (2021) 856–865.

[116] N.K. Wagh, D.-H. Kim, S.-H. Kim, S.S. Shinde, J.-H. Lee, Heuristic Iron–cobalt-mediated robust pH-Universal oxygen bifunctional lusters for reversible aqueous and flexible solid-state Zn–Air cells, ACS Nano 15 (2021) 14683–14696.

[117] W. Hong, E. Meza, C.W. Li, Controlling the Co–S coordination environment in Co-doped WS 2 nanosheets for electrochemical oxygen reduction, J. Mater. Chem. A 9 (2021) 19865–19873.

[118] Y. Xu, H. Zhang, P. Zhang, M. Lu, X. Xie, L. Huang, In situ exsolved Co components on wood ear-derived porous carbon for catalyzing oxygen reduction over a wide pH range, J. Mater. Chem. A 9 (2021) 10695–10703.

[119] N. Kumar, K. Naveen, M. Kumar, T.C. Nagaiah, R. Sakla, A. Ghosh, V. Siruguri, S. Sadhukhan, S. Kanungo, A.K. Paul, Multifunctionality exploration of Ca2FeRuO6: an efficient trifunctional electrocatalyst toward OER/ORR/HER and photocatalyst for water splitting, ACS Appl. Energy Mater. 4 (2021) 1323–1334.

[120] W. Liu, L. Zheng, S. Cheng, Y. Zhu, J. Sun, Cobalt-nitrogen-carbon nanotube co-implanted activated carbon as efficient cathodic oxygen reduction catalyst in microbial fuel cells, J. Electroanal. Chem. 876 (2020) 114498.

[121] R. Li, F.-Y. Zheng, X. Zhang, J. Hu, C. Xu, Y. Zhang, Phosphorus and iron doped nitrogen-containing carbon derived from biomass for oxygen reduction under various pH conditions, Int. J. Hydrogen Energy 45 (2020) 28651–28663.

[122] S.N. Chowdhury, S. Biswas, P. Das, S. Paul, A.N. Biswas, Oxygen reduction assisted by the concert of redox activity and proton relay in a Cu(II) complex, Inorg. Chem. 59 (2020) 14012–14022.

[123] X. Wang, Z. Zhang, H. Gai, Z. Chen, Z. Sun, M. Huang, An efficient pH-universal electrocatalyst for oxygen reduction: defect-rich graphitized carbon shell wrapped cobalt within hierarchical porous N-doped carbon aerogel, Mater. Today Energy 17 (2020) 100452.

[124] P.T. Smith, Y. Kim, B.P. Benke, K. Kim, C.J. Chang, Supramolecular tuning enables selective oxygen reduction catalyzed by cobalt porphyrins for direct electrosynthesis of hydrogen peroxide, Angew. Chem. 132 (2020) 4932–4937.

[125] J. Zhao, Z. Pu, H. Jin, Z. Zhang, J. Liu, S. Mu, Phosphorous-doped carbon coordinated iridium diphosphide bifunctional catalyst with ultralow iridium amount for efficient all-ph-value hydrogen evolution and oxygen reduction reactions, J. Catal. 383 (2020) 244–253.

[126] D. Wang, J. Hu, J. Yang, K. Xiao, S. Liang, J. Xu, B. Liu, H. Hou, Fe and N co-doped carbon derived from melamine resin capsuled biomass as efficient oxygen reduction catalyst for air-cathode microbial fuel cells, Int. J. Hydrogen Energy 45 (2020) 3163–3175.

[127] M. Muhyuddin, D. Testa, R. Lorenzi, G.M. Vanacore, F. Poli, F. Soavi, S. Specchia, W. Giurlani, M. Innocenti, L. Rosi, C. Santoro, Iron-based electrocatalysts derived from scrap tires for oxygen reduction reaction: evolution of synthesis-structure-performance relationship in acidic, neutral and alkaline media, Electrochim. Acta 433 (2022) 141254.

[128] D. Testa, G. Zuccante, M. Muhyuddin, R. Landone, A. Scommegna, R. Lorenzi, M. Acciarri, E. Petri, F. Soavi, L. Poggini, L. Capozzoli, A. Lavacchi, N. Lamanna, A. Franzetti, L. Zoia, C. Santoro, Giving new life to waste cigarette butts: transformation into platinum group metal-free electrocatalysts for oxygen reduction reaction in acid, neutral and alkaline environment, Catalysts 13 (2023) 635.

[129] P. Li, Y. Jiao, Y. Ruan, H. Fei, Y. Men, C. Guo, Y. Wu, S. Chen, Revealing the role of double-layer microenvironments in pH-dependent oxygen reduction activity over metal-nitrogen-carbon catalysts, Nat. Commun. 14 (2023) 6936.

[130] Y. Pang, H. Xie, Y. Sun, M.-M. Titirici, G.-L. Chai, Electrochemical oxygen reduction for H2O2 production: catalysts, pH effects and mechanisms, J. Mater. Chem. A 8 (2020) 24996–25016.

[131] M. Dan, R. Zhong, S. Hu, H. Wu, Y. Zhou, Z.-Q. Liu, Strategies and challenges on selective electrochemical hydrogen peroxide production: catalyst and reaction medium design, Chem Catal. 2 (2022) 1919–1960.

[132] Y. Bu, Y. Wang, G. Han, Y. Zhao, X. Ge, F. Li, Z. Zhang, Q. Zhong, J. Baek, Carbon-based electrocatalysts for efficient hydrogen peroxide production, Adv. Mater. 33 (2021) 2103266.

[133] E.I. Solomon, P. Chen, M. Metz, S.-K. Lee, A.E. Palmer, Oxygen binding, activation, and reduction to water by copper proteins, Angew. Chem. Int. Ed. 40 (2001) 4570–4590.

[134] A.E. Palmer, S.K. Lee, E.I. Solomon, Decay of the peroxide intermediate in laccase: reductive cleavage of the O− O bond, J. Am. Chem. Soc. 123 (2001) 6591–6599.

[135] W. Shin, U.M. Sundaram, J.L. Cole, H.H. Zhang, B. Hedman, K.O. Hodgson, E. I. Solomon, Chemical and spectroscopic definition of the peroxide-level intermediate in the multicopper oxidases: relevance to the catalytic mechanism of dioxygen reduction to water, J. Am. Chem. Soc. 118 (1996) 3202–3215.

[136] L. Quintanar, C. Stoj, A.B. Taylor, P.J. Hart, D.J. Kosman, E.I. Solomon, Shall we dance? How a multicopper oxidase chooses its electron transfer partner, Accounts Chem. Res. 40 (2007) 445–452.

[137] J. Yoon, B.D. Liboiron, R. Sarangi, K.O. Hodgson, B. Hedman, E.I. Solomon, The two oxidized forms of the trinuclear Cu cluster in the multicopper oxidases and mechanism for the decay of the native intermediate, Proc. Natl. Acad. Sci. 104 (2007) 13609–13614.

[138] J. Yoon, L.M. Mirica, T.D.P. Stack, E.I. Solomon, Variable-temperature, variable-field magnetic circular dichroism studies of tris-hydroxy-and μ3-oxo-bridged trinuclear Cu (II) complexes: evaluation of proposed structures of the native intermediate of the multicopper oxidases, J. Am. Chem. Soc. 127 (2005) 13680–13693.

[139] S. Calabrese Barton, J. Gallaway, P. Atanassov, Enzymatic biofuel cells for implantable and microscale devices, Chem. Rev. 104 (2004) 4867–4886.

[140] J. Tang, X. Yan, W. Huang, C. Engelbrekt, J.Ø. Duus, J. Ulstrup, X. Xiao, J. Zhang, Bilirubin oxidase oriented on novel type three-dimensional biocathodes with reduced graphene aggregation for biocathode, Biosens. Bioelectron. 167 (2020) 112500.

[141] W. Lipińska, V. Saska, K. Siuzdak, J. Karczewski, K. Załęski, E. Coy, A. de Poulpiquet, I. Mazurenko, E. Lojou, Interaction between bilirubin oxidase and Au nanoparticles distributed over dimpled titanium foil towards oxygen reduction reaction, Electrochim. Acta 474 (2024) 143535.

[142] G.C. Sedenho, A. Hassan, L.J.A. Macedo, F.N. Crespilho, Stabilization of bilirubin oxidase in a biogel matrix for high-performance gas diffusion electrodes, J. Power Sources 482 (2021) 229035.

[143] Á. Torrinha, M. Tavares, C. Delerue-Matos, S. Morais, Microenergy generation and dioxygen sensing by bilirubin oxidase immobilized on a nanostructured carbon paper transducer, Electrochim. Acta 445 (2023) 142061.
[144] M. Carrière, P. Henrique M. Buzzetti, K. Gorgy, F. Giroud, H. Li, R. Borsali, S. Cosnier, Nanostructured electrodes based on multiwalled carbon nanotube/glyconanoparticles for the specific immobilization of bilirubin oxidase: application to the electrocatalytic O2 reduction, Bioelectrochemistry 150 (2023) 108328.
[145] X. Xiao, D. Leech, J. Zhang, An oxygen-reducing biocathode with "oxygen tanks,", Chem. Commun. 56 (2020) 9767–9770.
[146] S. Nishida, H. Sumi, H. Noji, A. Itoh, K. Kataoka, S. Yamashita, K. Kano, K. Sowa, Y. Kitazumi, O. Shirai, Influence of distal glycan mimics on direct electron transfer performance for bilirubin oxidase bioelectrocatalysts, Bioelectrochemistry 152 (2023) 108413.
[147] S.R. Higgins, C. Lau, P. Atanassov, S.D. Minteer, M.J. Cooney, Hybrid biofuel cell: microbial fuel cell with an enzymatic air-breathing cathode, ACS Catal. 1 (2011) 994–997.
[148] C. Santoro, S. Babanova, P. Atanassov, B. Li, I. Ieropoulos, P. Cristiani, High power generation by a membraneless single chamber microbial fuel cell (SCMFC) using enzymatic bilirubin oxidase (BOx) air-breathing cathode, J. Electrochem. Soc. 160 (2013) H720.
[149] C. Santoro, S. Babanova, B. Erable, A. Schuler, P. Atanassov, Bilirubin oxidase based enzymatic air-breathing cathode: operation under pristine and contaminated conditions, Bioelectrochemistry 108 (2016) 1–7.
[150] M.C. Monteiro, M.T. Koper, Measuring local pH in electrochemistry, Curr. Opin. Electrochem. (2020) 100649.
[151] M. Bellare, V.K. Kadambar, P. Bollella, E. Katz, A. Melman, Electrochemically stimulated molecule release associated with interfacial pH changes, Chem. Commun. 55 (2019) 7856–7859.
[152] M. Bellare, V.K. Kadambar, P. Bollella, E. Katz, A. Melman, Molecular release associated with interfacial pH change stimulated by a small electrical potential applied, Chemelectrochem 7 (2020) 59–63.
[153] X. Xiao, K.D. McGourty, E. Magner, Enzymatic biofuel cells for self-powered, controlled drug release, J. Am. Chem. Soc. 142 (2020) 11602–11609.
[154] P. Bollella, A. Melman, E. Katz, Operando local pH mapping of electrochemical and bioelectrochemical reactions occurring at an electrode surface: effect of the buffer concentration, Chemelectrochem 8 (2021) 3923–3935.
[155] A. Tricase, B. Alhenaki, V. Marchianò, L. Torsi, R. Gupta, P. Bollella, Bioelectrochemically triggered apoferritin-based bionanoreactors: synthesis of CdSe nanoparticles and monitoring with leaky waveguides, Nanoscale Adv. 6 (2024) 516–523.
[156] M. Masi, P. Bollella, E. Katz, DNA release from a modified electrode triggered by a bioelectrocatalytic process, ACS Appl. Mater. Interfaces 11 (2019) 47625–47634.
[157] M. Masi, P. Bollella, O. Smutok, E. Katz, Photo-stimulated self-powered electrochemical system for DNA release, Sens. Acutators Rep. 3 (2021) 100058.
[158] M. Masi, P. Bollella, E. Katz, Biomolecular release stimulated by electrochemical signals at a very small potential applied, Electroanalysis 32 (2020) 95–103.
[159] P. Bollella, A. Melman, E. Katz, Electrochemically generated interfacial pH change: application to signal-triggered molecule release, Chemelectrochem 7 (2020), 3383–3383.
[160] T. Zeng, R.P. Gautam, D.H. Ko, H.-L. Wu, A. Hosseini, Y. Li, C.J. Barile, E.C. M. Tse, Hybrid bilayer membranes as platforms for biomimicry and catalysis, Nat. Rev. Chem 6 (2022) 862–880.
[161] K.-Y. Wang, J. Zhang, Y.-C. Hsu, H. Lin, Z. Han, J. Pang, Z. Yang, R.-R. Liang, W. Shi, H.-C. Zhou, Bioinspired framework catalysts: from enzyme immobilization to biomimetic catalysis, Chem. Rev. 123 (2023) 5347–5420, https://doi.org/10.1021/acs.chemrev.2c00879.
[162] A.C. Vilbert, Y. Liu, H. Dai, Y. Lu, Recent advances in tuning redox properties of electron transfer centers in metalloenzymes catalyzing the oxygen reduction reaction and H2 oxidation important for fuel cell design, Curr. Opin. Electrochem. 30 (2021) 100780.
[163] S. Kim, J. Ji, Y. Kwon, Paper-type membraneless enzymatic biofuel cells using a new biocathode consisting of flexible buckypaper electrode and bilirubin oxidase based catalyst modified by electrografting, Appl. Energy 339 (2023) 120978.
[164] N. Loew, I. Shitanda, H. Goto, H. Watanabe, T. Mikawa, S. Tsujimura, M. Itagaki, High-performance paper-based biocathode fabricated by screen-printing an improved mesoporous carbon ink and by oriented immobilization of bilirubin oxidase, Sci. Rep. 12 (2022) 14649.
[165] M. Miyata, K. Kano, O. Shirai, Y. Kitazumi, Rapid fabrication of nanoporous gold as a suitable platform for the direct electron transfer-type bioelectrocatalysis of bilirubin oxidase, Electrochemistry 88 (2020) 444–446.
[166] A.C. Dharmaratne, J.T. Moulton, J. Niroula, C. Walgama, S. Mazumder, S. Mohanty, S. Krishnan, Pyrenyl carbon nanotubes for covalent bilirubin oxidase biocathode design: should the nanotubes be carboxylated? Electroanalysis 32 (2020) 885–889.
[167] S. Liu, Z. Li, C. Wang, W. Tao, M. Huang, M. Zuo, Y. Yang, K. Yang, L. Zhang, S. Chen, Turning main-group element magnesium into a highly active electrocatalyst for oxygen reduction reaction, Nat. Commun. 11 (2020) 938.
[168] L. Dos Santos, V. Climent, C.F. Blanford, F.A. Armstrong, Mechanistic studies of the 'Blue'Cu enzyme, bilirubin oxidase, as a highly efficient electrocatalyst for the oxygen reduction reaction, Phys. Chem. Chem. Phys. 12 (2010) 13962–13974.
[169] V. Scotto, R. Di Cintio, G. Marcenaro, The influence of marine aerobic microbial film on stainless steel corrosion behaviour, Corros. Sci. 25 (1985) 185–194.
[170] A. Bergel, D. Féron, A. Mollica, Catalysis of oxygen reduction in PEM fuel cell by seawater biofilm, Electrochem. Commun. 7 (2005) 900–904.
[171] C. Santoro, C. Arbizzani, B. Erable, I. Ieropoulos, Microbial fuel cells: from fundamentals to applications. A review, J. Power Sources 356 (2017) 225–244.
[172] K. Guo, A. Prévoteau, S.A. Patil, K. Rabaey, Engineering electrodes for microbial electrocatalysis, Curr. Opin. Biotechnol. 33 (2015) 149–156.
[173] M. Rosenbaum, F. Aulenta, M. Villano, L.T. Angenent, Cathodes as electron donors for microbial metabolism: which extracellular electron transfer mechanisms are involved? Bioresour. Technol. 102 (2011) 324–333.
[174] B. Erable, D. Féron, A. Bergel, Microbial catalysis of the oxygen reduction reaction for microbial fuel cells: a review, ChemSusChem 5 (2012) 975–987.
[175] K. Rabaey, S.T. Read, P. Clauwaert, S. Freguia, P.L. Bond, L.L. Blackall, J. Keller, Cathodic oxygen reduction catalyzed by bacteria in microbial fuel cells, ISME J. 2 (2008) 519–527.
[176] Z. He, L.T. Angenent, Application of bacterial biocathodes in microbial fuel cells, Electroanalysis: An International Journal Devoted to Fundamental and Practical Aspects of Electroanalysis 18 (2006) 2009–2015.
[177] G.F. White, M.J. Edwards, L. Gomez-Perez, D.J. Richardson, J.N. Butt, T. A. Clarke, Mechanisms of bacterial extracellular electron exchange, Adv. Microb. Physiol. 68 (2016) 87–138.
[178] K.H. Nealson, B.M. Tebo, R.A. Rosson, Occurrence and mechanisms of microbial oxidation of manganese, in: Advances in Applied Microbiology, Elsevier, 1988, pp. 279–318. https://www.sciencedirect.com/science/article/pii/S0065216408702090. (Accessed 28 June 2024).
[179] Z. Lewandowski, H. Beyenal, Mechanisms of microbially influenced corrosion, in: H.-C. Flemming, P.S. Murthy, R. Venkatesan, K. Cooksey (Eds.), Marine and Industrial Biofouling, Springer Berlin Heidelberg, Berlin, Heidelberg, 2009, pp. 35–64.
[180] Y. Lekbach, T. Liu, Y. Li, M. Moradi, W. Dou, D. Xu, J.A. Smith, D.R. Lovley, Microbial corrosion of metals: the corrosion microbiome, in: Advances in Microbial Physiology, Elsevier, 2021, pp. 317–390. https://www.sciencedirect.com/science/article/pii/S0065291121000023. (Accessed 28 June 2024).
[181] K.-L. Yap, L.-N. Ho, S.-A. Ong, K. Guo, Y.-S. Oon, Y.-P. Ong, S.-H. Thor, Crucial roles of aeration and catalyst on caffeine removal and bioelectricity generation in a double chambered microbial fuel cell integrated electrocatalytic process, J. Environ. Chem. Eng. 9 (2021) 104636.
[182] S. Rahman, T. Jafary, A. Al-Mamun, M.S. Baawain, M.R. Choudhury, H. Alhaimali, S.A. Siddiqi, B.R. Dhar, A. Sana, S.S. Lam, Towards upscaling microbial desalination cell technology: a comprehensive review on current challenges and future prospects, J. Clean. Prod. 288 (2021) 125597.
[183] S. Prakash, K. Ponnusamy, S. Naina Mohamed, An insight on biocathode microbial desalination cell: current challenges and prospects, Intl J of Energy Research 46 (2022) 8546–8559.
[184] C. Santoro, C. Flores-Cadengo, F. Soavi, M. Kodali, I. Merino-Jimenez, I. Gajda, J. Greenman, I. Ieropoulos, P. Atanassov, Ceramic microbial fuel cells stack: power generation in standard and supercapacitive mode, Sci. Rep. 8 (2018) 1–12.
[185] L. Rago, P. Cristiani, F. Villa, S. Zecchin, A. Colombo, L. Cavalca, A. Schievano, Influences of dissolved oxygen concentration on biocathodic microbial communities in microbial fuel cells, Bioelectrochemistry 116 (2017) 39–51.
[186] R. Rossi, D. Jones, J. Myung, E. Zikmund, W. Yang, Y.A. Gallego, D. Pant, P. J. Evans, M.A. Page, D.M. Cropek, Evaluating a multi-panel air cathode through electrochemical and biotic tests, Water Res. 148 (2019) 51–59.
[187] M. Hoareau, B. Erable, O. Chapleur, C. Midoux, C. Bureau, A. Goubet, A. Bergel, Oxygen-reducing bidirectional microbial electrodes designed in real domestic wastewater, Bioresour. Technol. 326 (2021) 124663.
[188] M. Oliot, S. Galier, H. Roux de Balmann, A. Bergel, Ion transport in microbial fuel cells: key roles, theory and critical review, Appl. Energy 183 (2016) 1682–1704.
[189] M. Santini, S. Marzorati, S. Fest-Santini, S. Trasatti, P. Cristiani, Carbonate scale deactivating the biocathode in a microbial fuel cell, J. Power Sources 356 (2017) 400–407.
[190] M. Santini, M. Guilizzoni, M. Lorenzi, P. Atanassov, E. Marsili, S. Fest-Santini, P. Cristiani, C. Santoro, Three-dimensional X-ray microcomputed tomography of carbonates and biofilm on operated cathode in single chamber microbial fuel cell, Biointerphases 10 (2015) 031009.
[191] A. Janicek, Y. Fan, H. Liu, Design of microbial fuel cells for practical application: a review and analysis of scale-up studies, Biofuels 5 (2014) 79–92.
[192] S. Babanova, J. Jones, S. Phadke, M. Lu, C. Angulo, J. Garcia, K. Carpenter, R. Cortese, S. Chen, T. Phan, O. Bretschger, Continuous flow, large-scale, microbial fuel cell system for the sustained treatment of swine waste, Water Environ. Res. 92 (2020) 60–72.
[193] B.E. Logan, Scaling up microbial fuel cells and other bioelectrochemical systems, Appl. Microbiol. Biotechnol. 85 (2010) 1665–1671.
[194] P. Clauwaert, S. Mulenga, P. Aelterman, W. Verstraete, Litre-scale microbial fuel cells operated in a complete loop, Appl. Microbiol. Biotechnol. 83 (2009) 241–247.
[195] E. Blanchet, S. Pécastaings, B. Erable, C. Roques, A. Bergel, Protons accumulation during anodic phase turned to advantage for oxygen reduction during cathodic phase in reversible bioelectrodes, Bioresour. Technol. 173 (2014) 224–230.
[196] M. Rimboud, M. Barakat, A. Bergel, B. Erable, Different methods used to form oxygen reducing biocathodes lead to different biomass quantities, bacterial communities, and electrochemical kinetics, Bioelectrochemistry 116 (2017) 24–32.
[197] D.P.B.T.B. Strik, H.V.M. Hamelers, C.J.N. Buisman, Solar energy powered microbial fuel cell with a reversible bioelectrode, Environ. Sci. Technol. 44 (2010) 532–537.
[198] J.J. Villora-Picó, J. González-Arias, F.M. Baena-Moreno, T.R. Reina, Renewable carbonaceous materials from biomass in catalytic processes: a review, Materials 17 (2024) 565.

[199] D. Polidoro, A. Perosa, M. Selva, D. Rodríguez-Padrón, Metal-free carbonaceous catalytic materials: biomass feedstocks for a greener future, ChemCatChem 15 (2023) e202300415.
[200] K. Guo, S. Freguia, P.G. Dennis, X. Chen, B.C. Donose, J. Keller, J.J. Gooding, K. Rabaey, Effects of surface charge and hydrophobicity on anodic biofilm formation, community composition, and current generation in bioelectrochemical systems, Environ. Sci. Technol. 47 (2013) 7563–7570.
[201] C. Li, S. Cheng, Functional group surface modifications for enhancing the formation and performance of exoelectrogenic biofilms on the anode of a bioelectrochemical system, Crit. Rev. Biotechnol. 39 (2019) 1015–1030.
[202] A.P. Borole, G. Reguera, B. Ringeisen, Z.-W. Wang, Y. Feng, B.H. Kim, Electroactive biofilms: current status and future research needs, Energy Environ. Sci. 4 (2011) 4813–4834.
[203] A. Prévoteau, K. Rabaey, Electroactive biofilms for sensing: reflections and perspectives, ACS Sens. 2 (2017) 1072–1085.
[204] S.M. Strycharz-Glaven, R.H. Glaven, Z. Wang, J. Zhou, G.J. Vora, L.M. Tender, Electrochemical investigation of a microbial solar cell reveals a nonphotosynthetic biocathode catalyst, Appl. Environ. Microbiol. 79 (2013) 3933–3942.
[205] F. Smith, F. Brownlie, T. Hodgkiess, A. Toumpis, A. Pearson, A.M. Galloway, Effect of salinity on the corrosive wear behaviour of engineering steels in aqueous solutions, Wear 462 (2020) 203515.
[206] S.V. Nesterenko, Corrosion resistance of new duplex stainless steels in coke production, Coke Chem. 63 (2020) 88–96.
[207] W. Richard, B. Erable, A. Bergel, Whole cell (microbial) electrocatalysis of the oxygen reduction reaction (ORR), encyclopedia of interfacial chemistry, Surface Science and Electrochemistry 5 (2018) 920–929.
[208] W.S. da Cruz Nizer, M.E. Adams, K.N. Allison, M.C. Montgomery, H. Mosher, E. Cassol, J. Overhage, Oxidative stress responses in biofilms, Biofilm (2024) 100203.
[209] O.O. Kolajo, C. Pandit, B.S. Thapa, S. Pandit, A.S. Mathuriya, P.K. Gupta, D. A. Jadhav, D. Lahiri, M. Nag, V.J. Upadhye, Impact of cathode biofouling in microbial fuel cells and mitigation techniques, Biocatal. Agric. Biotechnol. 43 (2022) 102408.
[210] M.T. Noori, M.M. Ghangrekar, C.K. Mukherjee, B. Min, Biofouling effects on the performance of microbial fuel cells and recent advances in biotechnological and chemical strategies for mitigation, Biotechnol. Adv. 37 (2019) 107420.
[211] K. Scott, Microbial fuel cells: transformation of wastes into clean energy, in: Membranes for Clean and Renewable Power Applications, Elsevier, 2014, pp. 266–300. https://www.sciencedirect.com/science/article/pii/B9780857095459500100. (Accessed 29 June 2024).
[212] S.M. Tiquia-Arashiro, D. Pant, Microbial Electrochemical Technologies, CRC Press, Taylor & Francis Group, 2020. https://api.taylorfrancis.com/content/books/mono/download?identifierName=doi&identifierValue=10.1201/9780429487118&type=googlepdf. (Accessed 29 June 2024).
[213] A. Prévoteau, F.-M. Kerckhof, P. Clauwaert, K. Rabaey, Electrochemical and phylogenetic comparisons of oxygen-reducing electroautotrophic communities, Biosens. Bioelectron. 171 (2021) 112700.
[214] B. Erable, N.M. Duţeanu, M.M. Ghangrekar, C. Dumas, K. Scott, Application of electro-active biofilms, Biofouling 26 (2010) 57–71.
[215] A. Larrosa, L.J. Lozano, K.P. Katuri, I. Head, K. Scott, C. Godinez, On the repeatability and reproducibility of experimental two-chambered microbial fuel cells, Fuel 88 (2009) 1852–1857.
[216] S. Mateo, A. Cantone, P. Cañizares, F.J. Fernández-Morales, O. Scialdone, M. A. Rodrigo, Development of a module of stacks of air-breathing microbial fuel cells to light-up a strip of LEDs, Electrochim. Acta 274 (2018) 152–159.
[217] C. Santoro, S. Babanova, P. Cristiani, K. Artyushkova, P. Atanassov, A. Bergel, O. Bretschger, R.K. Brown, K. Carpenter, A. Colombo, R. Cortese, B. Erable, F. Harnisch, M. Kodali, S. Phadke, S. Riedl, L.F.M. Rosa, U. Schröder, How comparable are microbial electrochemical systems around the globe? An electrochemical and microbiological cross-laboratory study, ChemSusChem 14 (2021) 2313–2330.
[218] S. Debuy, S. Pecastaings, A. Bergel, B. Erable, Oxygen-reducing biocathodes designed with pure cultures of microbial strains isolated from seawater biofilms, Int. Biodeterior. Biodegrad. 103 (2015) 16–22.
[219] B. Erable, I. Vandecandelaere, M. Faimali, M.-L. Delia, L. Etcheverry, P. Vandamme, A. Bergel, Marine aerobic biofilm as biocathode catalyst, Bioelectrochemistry 78 (2010) 51–56.
[220] E.M. Conners, K. Rengasamy, A. Bose, Electroactive biofilms: how microbial electron transfer enables bioelectrochemical applications, J. Ind. Microbiol. Biotechnol. 49 (2022) kuac012.
[221] M.D. Yates, B.J. Eddie, N.J. Kotloski, N. Lebedev, A.P. Malanoski, B. Lin, S. M. Strycharz-Glaven, L.M. Tender, Toward understanding long-distance extracellular electron transport in an electroautotrophic microbial community, Energy Environ. Sci. 9 (2016) 3544–3558.
[222] J.M. Sonawane, S. Gupta, D. Pant, Microbial electrosynthesis for bio-based production using renewable electricity. https://books.rsc.org/books/edited-volume/1451/chapter/953395, 2021. (Accessed 29 June 2024).
[223] X.-W. Liu, W.-W. Li, H.-Q. Yu, Cathodic catalysts in bioelectrochemical systems for energy recovery from wastewater, Chem. Soc. Rev. 43 (2014) 7718–7745.
[224] T.J.-P. Ivase, B.B. Nyakuma, O. Oladokun, P.T. Abu, M.N. Hassan, Review of the principal mechanisms, prospects, and challenges of bioelectrochemical systems, Environ. Prog. Sustain. Energy 39 (2020) 13298.
[225] X.X. Wang, M.T. Swihart, G. Wu, Achievements, challenges and perspectives on cathode catalysts in proton exchange membrane fuel cells for transportation, Nat. Catal. 2 (2019) 578–589.
[226] E.B. Estrada-Arriaga, O. Guadarrama-Pérez, S. Silva-Martínez, C. Cuevas-Arteaga, V.H. Guadarrama-Pérez, Oxygen reduction reaction (ORR) electrocatalysts in constructed wetland-microbial fuel cells: effect of different carbon-based catalyst biocathode during bioelectricity production, Electrochim. Acta 370 (2021) 137745.
[227] Y. Wei, Y. Jiao, D. An, D. Li, W. Li, Q. Wei, Review of dissolved oxygen detection technology: from laboratory analysis to online intelligent detection, Sensors 19 (2019) 3995.
[228] S. Babanova, K. Artyushkova, Y. Ulyanova, S. Singhal, P. Atanassov, Design of experiments and principal component analysis as approaches for enhancing performance of gas-diffusional air-breathing bilirubin oxidase cathode, J. Power Sources 245 (2014) 389–397.
[229] C. Santoro, X.A. Walter, F. Soavi, J. Greenman, I. Ieropoulos, Air-breathing cathode self-powered supercapacitive microbial fuel cell with human urine as electrolyte, Electrochim. Acta 353 (2020) 136530.
[230] J.C. Kurnia, B.A. Chaedir, A.P. Sasmito, T. Shamim, Progress on open cathode proton exchange membrane fuel cell: performance, designs, challenges and future directions, Appl. Energy 283 (2021) 116359.
[231] S.B. Adler, Factors governing oxygen reduction in solid oxide fuel cell cathodes, Chem. Rev. 104 (2004) 4791–4844.
[232] I. Merino-Jimenez, C. Santoro, S. Rojas-Carbonell, J. Greenman, I. Ieropoulos, P. Atanassov, Carbon-based air-breathing cathodes for microbial fuel cells, Catalysts 6 (2016) 127.
[233] S. Srikanth, D. Pant, X. Dominguez-Benetton, I. Genné, K. Vanbroekhoven, P. Vermeiren, Y. Alvarez-Gallego, Gas diffusion electrodes manufactured by casting evaluation as air cathodes for microbial fuel cells (MFC), Materials 9 (2016) 601.
[234] P. Ledezma, A. Stinchcombe, J. Greenman, I. Ieropoulos, The first self-sustainable microbial fuel cell stack, Phys. Chem. Chem. Phys. 15 (2013) 2278–2281.
[235] S.B. Pasupuleti, S. Srikanth, X. Domínguez-Benetton, S.V. Mohan, D. Pant, Dual gas diffusion cathode design for microbial fuel cell (MFC): optimizing the suitable mode of operation in terms of bioelectrochemical and bioelectro-kinetic evaluation, J. Chem. Technol. Biotechnol. 91 (2016) 624–639.
[236] K.P. Katuri, S. Kalathil, A. Ragab, B. Bian, M.F. Alqahtani, D. Pant, P.E. Saikaly, Dual-function electrocatalytic and macroporous hollow-fiber cathode for converting waste streams to valuable resources using microbial electrochemical systems, Adv. Mater. 30 (2018) 1707072.
[237] H. Hiegemann, T. Littfinski, S. Krimmler, M. Lübken, D. Klein, K.-G. Schmelz, K. Ooms, D. Pant, M. Wichern, Performance and inorganic fouling of a submergible 255 L prototype microbial fuel cell module during continuous long-term operation with real municipal wastewater under practical conditions, Bioresour. Technol. 294 (2019) 122227.
[238] Spark of life - teresa van dongen, (n.d.). http://www.teresavandongen.com/Spark-of-Life (accessed July 12, 2020).
[239] D. Pant, A. Singh, G. Van Bogaert, S.I. Olsen, P.S. Nigam, L. Diels, K. Vanbroekhoven, Bioelectrochemical systems (BES) for sustainable energy production and product recovery from organic wastes and industrial wastewaters, RSC Adv. 2 (2012) 1248–1263.
[240] T. Wilberforce, E.T. Sayed, M.A. Abdelkareem, K. Elsaid, A.G. Olabi, Value added products from wastewater using bioelectrochemical systems: current trends and perspectives, J. Water Proc. Eng. 39 (2021) 101737.
[241] A. Dodón, V. Quintero, M. Chen Austin, D. Mora, Bio-inspired electricity storage alternatives to support massive demand-side energy generation: a review of applications at building scale, Biomimetics 6 (2021) 51.
[242] R. Paul, Q. Dai, C. Hu, L. Dai, Ten years of carbon-based metal-free electrocatalysts, Carbon Energy 1 (2019) 19–31.
[243] P. Bollella, Y. Hibino, K. Kano, L. Gorton, R. Antiochia, Enhanced direct electron transfer of fructose dehydrogenase rationally immobilized on a 2-aminoanthracene diazonium cation grafted single-walled carbon nanotube based electrode, ACS Catal. 8 (2018) 10279–10289.
[244] S. Igarashi, T. Hirokawa, K. Sode, Engineering PQQ glucose dehydrogenase with improved substrate specificity: site-directed mutagenesis studies on the active center of PQQ glucose dehydrogenase, Biomol. Eng. 21 (2004) 81–89.
[245] J. Ni, L. Li, Cathode architectures for rechargeable ion batteries: progress and perspectives, Adv. Mater. 32 (2020) 2000288.
[246] P. Vensaus, Y. Liang, J.-P. Ansermet, G.J. Soler-Illia, M. Lingenfelder, Enhancement of electrocatalysis through magnetic field effects on mass transport, Nat. Commun. 15 (2024) 2867.